August 2024
Report No. 24-061

**Maura Healey**
Governor
**Kim Driscoll**
Lieutenant Governor
**Monica Tibbits-Nutt**
MassDOT Secretary & CEO

# Development of Improved Inspection Techniques Using LiDAR for Deteriorated Steel Beam Ends

Principal Investigator (s)
Simos Gerasimidis
Chengbo Ai
Sergio Brena

University of Massachusetts Amherst

Research and Technology Transfer Section
MassDOT Office of Transportation Planning

U.S. Department of Transportation
Federal Highway Administration

[This blank, unnumbered page will be the back of your front cover]

# Technical Report Document Page

| | | |
|---|---|---|
| 1. Report No.<br>24-061 | 2. Government Accession No. | 3. Recipient's Catalog No. |
| 4. Title and Subtitle<br>Development of Improved Inspection Techniques Using LiDAR for Deteriorated Steel Beam Ends | | 5. Report Date<br>August 2024<br>6. Performing Organization Code<br>24-061 |
| 7. Author(s)<br>Aidan Provost, Simos Gerasimidis, Chengbo Ai, Sergio Breña | | 8. Performing Organization Report No. |
| 9. Performing Organization Name and Address<br>University of Massachusetts Amherst, UMass Transportation Center, 130 Natural Resources Way, Amherst, MA 01003 | | 10. Work Unit No. (TRAIS)<br>11. Contract or Grant No. |
| 12. Sponsoring Agency Name and Address<br>Massachusetts Department of Transportation<br>Office of Transportation Planning<br>Ten Park Plaza, Suite 4150, Boston, MA 02116 | | 13. Type of Report and Period Covered<br>Final Report - August 2024 (March 2022 - August 2024)<br>14. Sponsoring Agency Code<br>n/a |
| 15. Supplementary Notes<br>Project Champion - Jean Marauszwski, MassDOT | | |

16. Abstract

This report summarizes the research on enhancing the current inspection protocols for MassDOT using 3D scanning technologies. The first part of the report presents a thorough review of the current methods using 3D scanning techniques for bridge inspection. The report also includes laboratory and field scans on corroded beam ends. The research team used different scanning techniques, scanning technologies, and post-processing techniques to find the method that would yield the most accurate result and be the most implementable by the DOT. Part of the presented research was to develop and validate a semiautomated point cloud data/scanning extraction method. Finally, the research team developed a method for 3D scanning to be used in bridge inspection. The main goal of the project is presented at the end of the report and consists of a comprehensive and implementable protocol for 3D-scanning-enriched bridge inspection.

| | | | |
|---|---|---|---|
| 17. Key Word<br>LiDAR, deteriorated steel beam ends, 3D scanning, technology, bridge inspections, bridges | 18. Distribution Statement | | |
| 19. Security Classif. (of this report)<br>unclassified | 20. Security Classif. (of this page)<br>unclassified | 21. No. of Pages<br>83 | 22. Price<br>n/a |

**Form DOT F 1700.7** (8-72) Reproduction of completed page authorized

This page left blank intentionally.

# Development of Improved Inspection Techniques Using LiDAR for Deteriorated Steel Beam Ends

Final Report

Prepared By:

**Aidan Provost**
Ph.D. Candidate and
Graduate Researcher
aqprovost@umass.edu

**Simos Gerasimidis, Ph.D.**
Principal Investigator
sgerasimidis@umass.edu

**Sergio Breña, Ph.D.**
Principal Investigator
brena@umass.edu

**Chengbo Ai, Ph.D.**
Principal Investigator
chengbo.ai@umass.edu

University of Massachusetts Amherst,
130 Natural Resources Way, Amherst, MA 01003

Prepared For:

Massachusetts Department of Transportation Office of Transportation Planning
Ten Park Plaza, Suite 4150 Boston, MA 02116

August 2024

This page left blank intentionally.

# Acknowledgments

Prepared in cooperation with the Massachusetts Department of Transportation, Office of Transportation Planning, and the United States Department of Transportation, Federal Highway Administration.

The Project Team would like to acknowledge the efforts of Mark Gauthier for all of his work and dedication to the lab spaces and to this project specifically with the experiments being performed at the University of Massachusetts Amherst. The research team would also like to thank MassDOT, Gill Engineering, and CHA/CME for their support and efforts to contribute to the field work conducted throughout this project. Finally, the research team would like to thank the Source Graphics/Artec 3D support team for helping with the initial setup and problem-solving techniques with the handheld scanner and commercial software.

# Disclaimer

This page left blank intentionally.

# Executive Summary

This study of Development of Improved Inspection Techniques Using LiDAR for Deteriorated Steel Beam Ends was undertaken as part of the Massachusetts Department of Transportation (MassDOT) Research Program. This program is funded with Federal Highway Administration (FHWA) State Planning and Research (SPR) funds. Through this program, applied research is conducted on topics of importance to the Commonwealth of Massachusetts transportation agencies.

The following report is the research product of the project conducted to enhance the current inspection protocols for the Massachusetts Department of Transportation via advanced technologies in 3D scanning. The first phase of this project was to conduct a rigorous review of the current methods using 3D scanning techniques for bridge inspection. This literature review served as a foundation for the research methodologies ultimately created and implemented by the researchers in this study. Following the literature review, the research team conducted laboratory and field scans on corroded beam ends. For this work, the researchers used different scanning techniques, scanning technologies, and post-processing techniques to find the method that would yield the most accurate result and be the most implementable by the Department of Transportation. Task 4 of the project was to develop and validate a semiautomated point cloud data/scanning extraction method. This task was simultaneously conducted alongside the scanning and post-processing of Tasks 2 and 3. Task 5 was to develop a method for 3D scanning to be used in bridge inspection. This was the main goal of the project; it serves as a summary to the methods of the research conducted and most importantly serves as a comprehensive and implementable protocol for 3D-scanning-enriched bridge inspection.

This page left blank intentionally.

# Table of Contents

# List of Tables



# List of Figures

This page left blank intentionally.

# List of Acronyms

| Acronym | Expansion |
|---|---|
| LiDAR | Light Detection and Ranging |
| SfM | Structure-from-Motion |
| ICP | Iterative Closest Point |
| BHM | Bridge Health Monitoring |
| LVDT | Linear Variable Differential Transformer |
| UAV | Unmanned Aerial Vehicle |
| ASCE | American Society of Civil Engineers |
| - | - |
| - | - |
| - | - |
| - | - |
| - | - |
| - | - |
| - | - |
| - | - |
| - | - |
| - | - |
| - | - |
| - | - |
| - | - |
| - | - |
| - | - |
| - | - |
| - | - |
| - | - |
| - | - |
| - | - |
| - | - |
| - | - |
| - | - |

This page left blank intentionally.

# 1.0 Introduction

Bridge inspection is a task that must be consistently performed on the nation's structures to ensure structural efficiency and, most importantly, public safety. ASCE has stated that 7.5% of the bridges nationwide are considered "structurally deficient." This poses a great challenge to engineers and agencies nationally *(1)*.

In New England specifically, significant deterioration due to corrosion has been observed by bridge inspectors. Approximately 72% of New England's 10,155 steel bridges are currently labelled as "Fair" or "Poor" condition rating, a number that will continue to rise with increasing structural age, the recurrent freeze-thaw cycles, and deicing techniques *(2)*. Corrosion is the main deleterious factor for steel bridges.

The corrosion exhibited on steel structures can often be found at the ends of the beams at the abutments; this is where water, deicing chemicals, and other debris can pass through expansion joints from the deck to the superstructure below. As this process repeats, corrosion wears away at the girder thus reducing the load-carrying capacity of the structural member. Inspecting and documenting the damage due to corrosion is a difficult task where rust is removed from a beam's surface and the inspector takes point measurements and makes visual assessments. While this is common practice, access to the beam ends can be difficult for inspectors to clean and to use these tools. Furthermore, point measurement tools provide limited information and can be temperamental if the steel surface is not fully cleaned or if there are many surface defects such as pitting.

The research summarized in the following report aspires to create a more comprehensive protocol in bridge inspecting by means of innovative technologies like LiDAR and photogrammetric 3D scanners. To accomplish this goal, the research project was split into six different tasks listed below in Table 1.1.

**Table 1.1: Project task outline**

| Task # | Description of work |
|---|---|
| **Task 1** | Review of LiDAR-based bridge inspection methods and practices |
| **Task 2** | Lab experiments for residual capacity estimation |
| **Task 3** | Field experiments for residual capacity estimation |
| **Task 4** | Develop and validate the automated or semiautomated LiDAR point cloud extraction method |
| **Task 5** | Develop a new protocol for LiDAR-enriched bridge inspection |
| **Task 6** | Research report and project deliverables |

This final report serves as the final task of the six tasks listed above in Table 1.1: Project task outline

.1. The first of these tasks was to perform an extensive review of the current methods and practices for which 3D scanning has been used in the bridge inspection process. In tasks two and three of this project, the research team selected beams to be scanned in the Brack Structural Engineering Laboratory at the University of Massachusetts–Amherst and on the selected highway bridge in Springfield, Massachusetts. From the scans performed in these respective groups, the research team was able to improve and develop a processing pipeline and protocol for to enhance bridge inspection via 3D scanning techniques.

# 2.0 Literature Review

## 2.1 Introduction

The first task consisted of a rigorous review of the current methods of bridge inspection that use 3D scanning technologies. To perform this task effectively, the research team had to consider the background and foundation of LiDAR and photogrammetry to understand their principles and how they could be applied to the field of structural inspection. Next, the research team considered different uses of LiDAR and photogrammetry within the field of structural inspection, which included capture methods, effective practices, and global inspection of bridge structures. Following the work in global inspection, research in corroded steel beam capacity estimation and corroded beam documentation via scanning were summarized as these are the major foundational research areas for the current study. Finally, the research team discussed the errors in scanning observed across the multitude of scanning methods and applications covered in the research from background to application. The following literature review aims to be a study in the field of 3D scanning particularly in the realm of structural deterioration and inspection.

## 2.2 LiDAR: Background

The term LiDAR was first coined in 1953 with ideas and fundamental techniques dating as far back as the 1930s *(3, 4, 5)*. In this time, the baseline techniques were performed on the atmosphere and clouds via the use of searchlights *(5-9)*. Elterman was able to extract height data using a telescope and measurements along such a light beam via the receiver field of view *(3,4,10)*. Throughout much of the early stages and development of LiDAR, the methods above were commonly used in meteorology. Middleton and Spilhaus were the researchers who first used the term LiDAR to describe the process for closed-loop, or "round-trip," measurements of height data via the time "between pulse emission and signal detection" *(3,4,5)*. In 1960, the development of the laser greatly impacted and improved the optical technology from the previous methods using searchlights and other illumination techniques *(3,4,11)*. Maiman's observations with ruby and a high-power flash lamp resulted in the creation of the laser that would ultimately lead to the development of modern LiDAR units; measuring the emissions and reception of laser pulses is the basis of the current technologies *(11)*.

Wandinger discusses the fundamentals of what composes a LiDAR system; that at its basis, a LiDAR system is a transmitter and a receiver *(3,4)*. The transmitter sends light pulses that have specified spectra properties pertaining to the light emitted by the laser *(3,4)*. On the receiving end, there is a telescope that gathers the returning photons, which are analyzed via an "optical analyzing system" where "selected radiation" is transmitted to a detector to be converted from optical to electrical data signals *(3,4)*. Ultimately, the time between the

transmission and reception of the laser data translates to “intensity of the signal” *(3,4)*. This process described by Wandinger is visualized in the graphic in Figure 2.1 below *(3)*.

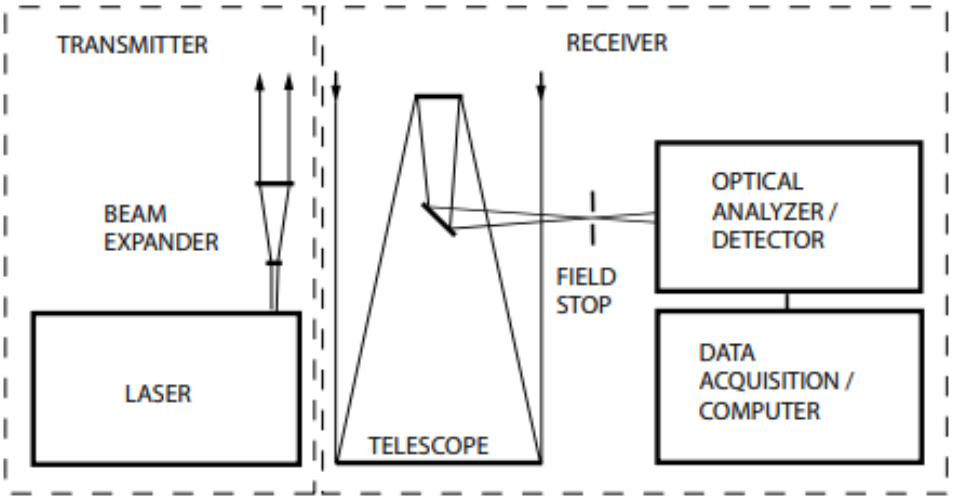


**Figure 2.1: Conceptural setup of lidar system from Wandinger *(3)***

There have been significant developments in the multitude of LiDAR technologies that have flourished following the creation of the laser and development of the LiDAR concept. The equipment that is currently available in today’s market spans LiDAR units that can be mounted on drones, larger terrestrial LiDAR scanners, and even LiDAR onboard smartphones such as the iPhone *(12)*. Each of these scanners has a variety of applications and accuracy and have a significant range in cost. For example, the iPhone 15 Pro Max costs $1199 dollars but does not currently have the accuracy or range of the terrestrial Riegl scanners, which could cost hundreds of thousands of dollars depending on the unit chosen *(12,13)*. Examples of current LiDAR units on the market can be found in Figure 2.2 below.


(a)Apple iPhone 15 Pro Max *(12)*, (b) RIEGL VUX-240 *(13)*, (c) RIEGL VZ-2000i *(13)*.

**Figure 2.2: LiDAR Scanning Tools**

## 2.3 Photogrammetry: Background

Photogrammetry, or the first photogrammetry system (system referring to a camera and a procedure for photogrammetry), was created in the 1700s by Aimé Laussedat, who has been called the "father of photogrammetry" *(14)*. With progressive and drastic improvements in photogrammetry technology, which includes cameras, techniques, and scanners, the applications have also drastically grown and developed over time. While this is the case, the basic concepts and fundamentals of photogrammetry have stayed the same at their core *(14)*. Linder explains the key difference between one photo, which is a two-dimensional plane of information, and finding a way to obtain the third dimension *(15)*. The solution is called "stereoscopic viewing," in which two or more photos are taken of the same object in different positions *(15)*.

Fundamentally, Linder defines the main goal of photogrammetry as the following: "For any object point represented in at least two photos we have to calculate the three-dimensional object (terrain) coordinates" *(15)*. The principles behind the photogrammetry process using an aerial photogrammetry example provided by Linder are shown in Figure 2.3 *(15)*. Alongside this, Schenk describes the data acquisition of photogrammetry as "obtaining reliable information about the properties of surfaces and objects" and is "accomplished without physical contact with the objects" *(16)*.

The basis of data acquisition for photogrammetry is described in this list from Schenk:

- "Geometric information: involves the spatial position and the shape of objects. It is the most important information source in photogrammetry"
- "Physical Information refers to properties of electromagnetic radiation, e.g., radiant energy, wavelength, and polarization"
- "Semantic information is related to the meaning of an image. It is usually obtained by interpreting the recorded data"
- "Temporal information is related to the change of an object in time, usually obtained by comparing several images which were recorded at different times" *(16)*.

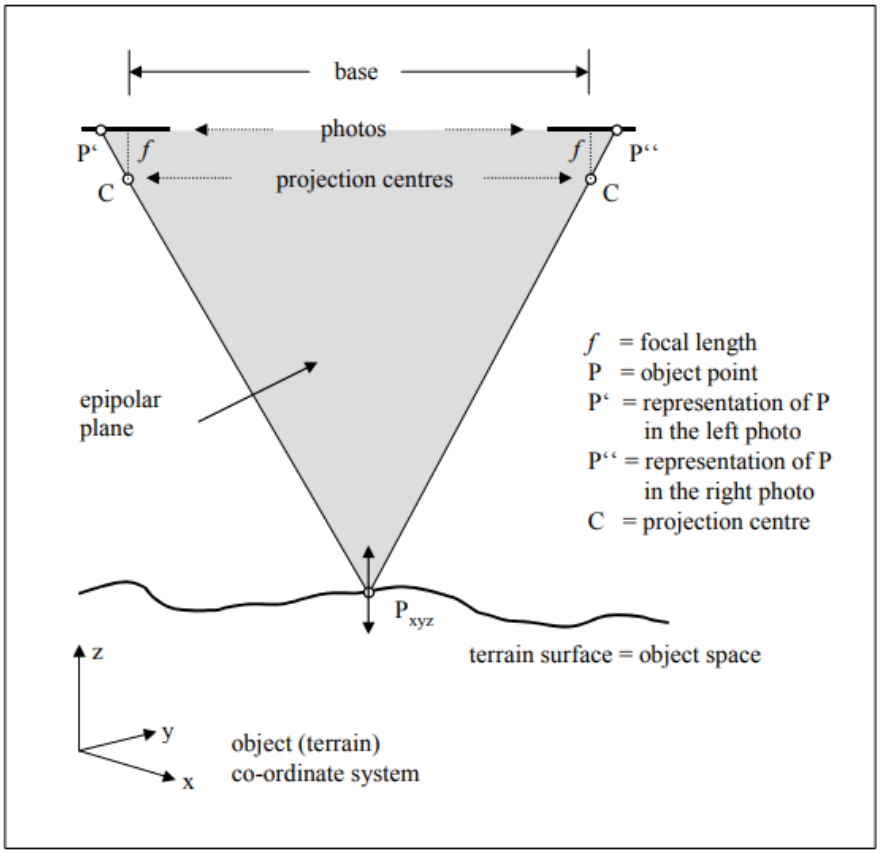


Changing the height in point P (on the surface) leads to a linear motion (left–right) of the points P' and P'
From Linder *(15)*

**Figure 2.3: Geometry in an oriented stereo model within photos along epipolar lines**

The figure above shows how an "object point" is found within at least two photos in the photogrammetry process *(15)*. Linder describes how, using the concept described above, if it

is possible for the photographed/scanned object to be recreated or if there is known geometric information, the user can estimate the three-dimensional coordinates and their overlap *(15)*.

As the applications of photogrammetry have increased, defining branches of photogrammetry have been used to subdivide the methodology for specific tasks and practice. Jauregui clearly describes the distinction between interpretive (or qualitative) and metric (or quantitative) photogrammetry *(14)*. Metric photogrammetry in particular can be subdivided into two primary categories: aerial and terrestrial *(14)*. According to Jauregui, aerial photogrammetry is often associated with land topology mapping and land surveying, and has applications in highway design *(14)*. Additionally, Jauregui explains that terrestrial photogrammetry, while having a vast measurement distance range of approximately 4 inches to 330 feet, is different than its aerial counterpart because it uses camera stations and its captures typically take place from the sides rather than from a bird's-eye view above *(14)*.

With a large range of photogrammetry applications and methodologies, the equipment that is currently available in today's market has expanded greatly since photogrammetry's first use. Because photogrammetry at its foundation relies heavily on image overlap and stitching, the hardware that can be used to perform photogrammetric techniques can span cellular devices to DSLR cameras, or even be imbedded into handheld scanners. Additionally, drones or unmanned aerial vehicles can be outfitted with cameras to perform photo capture for photogrammetry. Two examples of devices that can capture data for photogrammetry, an EOS Rebel T7 EF-S 18-55mm IS II camera and the Artec LEO Scanner, are shown in Figure 2.4 below *(17, 18)*.


(a) EOS Rebel T7 EF-S 18-55mm IS II *(17)* (b) Artec LEO Scanner *(18)*

**Figure 2.4: Photogrammetry data capture devices**

Many photogrammetry techniques use a camera with registration points or a rig system. The Artec Leo scanner automatically performs the stitching of photographs as it scans an object *(18)*.

## 2.4 LiDAR and Photogrammetry: Comparison

Many researchers have investigated photogrammetry and LiDAR across multiple disciplines. In the field of civil engineering, and specifically bridge inspection, many researchers have used scanning for the global structure or elemental geometry within the structure *(20, 21,22)*. This refers to the elements such as beam geometry, decks, and piers or even the entire structure. Many of these applications can be considered close-range photogrammetry, where the system is within the range of 4 inches to 330 feet of the object being captured *(14,23)*.

Prior to the use of photogrammetric scanners, researchers would use many types of cameras to capture the desired surfaces and create 3D renderings in several types of computer programs such as PhotoModeler software, Australis systems, Agisoft PhotoScan Pro software, and various other photogrammetric software *(20,24-26)*. Similarly, various point cloud software has been used to visualize and process data taken from various LiDAR scanners that have been outfitted on drone machinery. Molina performed measurements for bridge structure inspection in a direct comparison between photogrammetry, LiDAR units, and the original bridge plans to analyze global geometry and found that both scanning methods performed with low error *(27)*.

Linder discusses the advantage of LiDAR when objects that are being scanned have a lack of or very low texture, a trait that is critical for photogrammetry to perform well *(15)*. Linder also expressed that while this is a major advantage for LiDAR versus the use of photogrammetry, at the time LiDAR scanning was "very expensive," "time-consuming," and that "laser scanning cannot be used for fast moving objects" *(15)*. While there are still fundamental challenges and drawbacks to each method, today there is a vast market of 3D scanners and applications for which both photogrammetry and LiDAR are competitive solutions. Overall, the use of 3D scanning has higher data processing time with a lower cost and more information or data gathered *(24)*. While employing these methodologies, many researchers have investigated their use for large structural inspection, such as in bridges.

## 2.5 LiDAR and Photogrammetry: Unmanned Arial

Many other researchers have paired the use of LiDAR and photogrammetry with Unmanned Aerial Vehicles (UAVs) or drone machinery. Bolourian et al. *(28, 29,30)*, Jung et al. *(31,32)*, Zollini et al. *(24)*, Chen et al. *(33)*, Mohammadi et al. *(21)*, Molina et al. *(27)*, Hackl et al. *(26)*, and Perry et al. *(34)* have all employed UAVs outfitted with LiDAR sensors for bridge inspection. A key concept highlighted by many researchers is the concept of path planning for scanning with these UAV devices; this includes prioritizing areas that are considered critical or controlling sections of the structure with damage that must be captured and designing a flight that minimizes time and cost while maximizing the amount of data captured *(31)*. Ultimately, the data gathered using this equipment is vital in documenting

deterioration but can also be used to create a 3D model, or what is commonly referred to as a "digital twin" of the structure being captured. In practice, there are many drones across the market that allow for LiDAR units, cameras, or other recording equipment to be mounted to the drone system for scanning or photography. There are also select companies such as DJI, which has drones outfitted with RGB cameras and multispectral cameras for scanning, and Wingtra, which has drones outfitted with cameras and systems for photogrammetry and even for thermal imaging *(35, 36).* An example of a DJI drone with an embedded multispectral camera system is shown in Figure 2.5 *(35)*.

**Figure 2.5. The DJI P4 Multispectral Drone *(35)***

## 2.6 Scan Quality and Analysis

When 3D scanning is employed, there are many critical needs to ensure the data correctly represents the scanned object or structure and to ensure the scan quality is sufficient. Bolourian et al. emphasize the criticality of quality scanning particularly in the discussion of "overlaps," or overlapping surfaces shared between scans *(28, 29, 30)*. Overlaps, or at least overlapping reference points, are a necessity in the alignment and registration process; surfaces with overlapping data ultimately provide higher-density clouds for that particular area *(28, 29,30)*. For the registration process, in the case of point clouds in particular, excessive overlaps can result in errors in the form of "overfitting" *(28, 29,30)*. Moreover, Arun and Besl discuss alignment via point picking and the iterative closest point method (ICP), which result in a translation and rotation matrix *(37, 38)*. Additionally, Mohammadi discusses the importance of alignment, the transformation matrix, and the use of ICP in the application of scanning and evaluating the quality of digital twins *(21)*. The transformation matrix ultimately describes the resulting alignment necessary to bring a scan into the same coordinate space as the other. Having accurate measurement and alignment methods in the field of 3D scanning is critical in creating high-fidelity models to represent structures and structural members.

## 2.7 Scanning Methodologies and Applications for Infrastructure Deterioration

A common use of scanning technology in bridge infrastructure has been for larger, global changes in the structure, such as deflection of the bridge or bridge members due to loading. Jiang *(25)* discusses how several researchers have investigated deflection and failure in structural members via photogrammetric techniques; the members and failure methods discussed included buckling in steel girder flanges, crack detection, column deflection, and concrete beam deflection. Bales used photogrammetry for measuring beam deflections within bridge structures *(39)*. It is also important to note Bales's use of targets with distinguishable corners and center points to be used as control points in the monitoring process. The use of target points and surfaces is a common technique employed across many photogrammetric and LiDAR scanning methodologies. Cooper employed photogrammetry for use on the monitoring of steel bridge deformations *(40)*. In this study, the use of target points was once again employed, this time using 3M Scotchlite retroreflective sheeting with circular targets and numbering *(40)*. Target points for control measurements are imperative for accurate registration, stitching, and recreation of a scanned or photographed object. The target points used by Bales and Cooper can be found in Figure 2.6 *(39, 40)*.

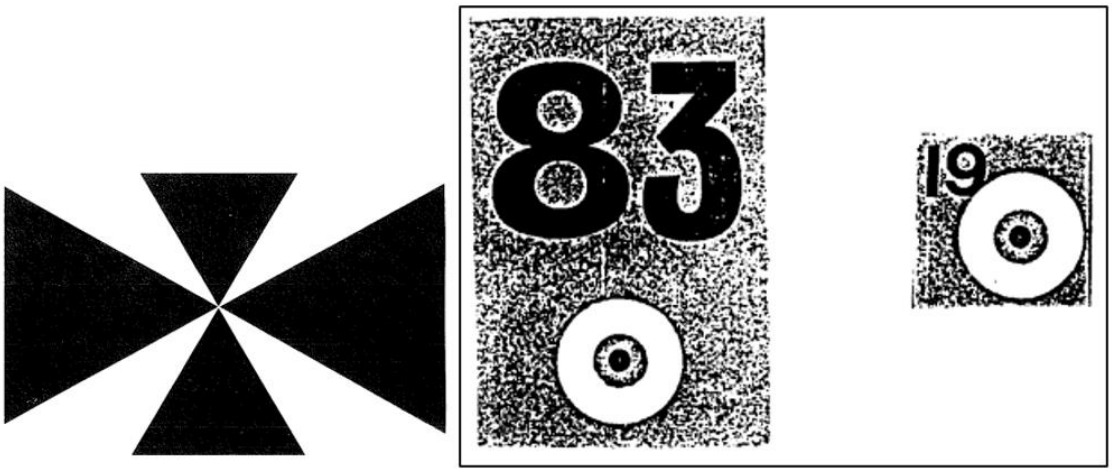


(a) (b)

(a) Targets used to mark horizontal and vertical control positions, Bales *(39)*

(b) Large and small retroreflective targets at full size, Cooper *(40)*

**Figure 2.6: Target points**

The target points above were used as control points in the photogrammetry process. Bales and Cooper both used control points to assist in the measurement of deflection; both considered the larger structure and were concerned with deflection *(39, 40)*.

The work of Bales and Cooper specifically pertain to bridge deflections; there are other studies for which photogrammetry and the use of target points were applied *(39, 40)*. Fraser

and Whiteman conducted studies using photogrammetry and employed the use of target points within their experimental work *(41, 42)*. The studies that Whiteman conducted on deflections in concrete beams also employed the idea of control points on a static surface and deforming targets on a concrete beam specimen *(42)*. Whiteman showed through the experimental destructive testing of concrete beams that a photogrammetric network achieved "sub-millimeter object point precision" and could outperform contact sensors such as LVDTs *(42)*. A key finding from Whiteman was through direct comparison of photogrammetry and LVDTs; there was good agreement between the two methods and while this was the case, it was made clear that there was great weakness in the conventional contact sensors such as "limited range, non-linearity in response and the ability to measure only in one dimension" *(42)*. It was apparent that through these studies, photogrammetry methods allowed Whiteman to gather more information about the concrete beam behavior throughout the experimental tests *(42)*.

In the work done by Fraser, a photogrammetric network was also established to measure thermal deformation of steel beams for which seven steel beams were successfully measured. The steel during these experiments were of temperatures around 1100 degrees Celsius, an environment in which it is extremely difficult to measure deflection by conventional hand tools *(41)*. By conducting these tests, Fraser states how photogrammetry, and "vision metrology" in general, can be used in these kinds of more severe or critical environments *(41)*. This key observation directly relates to 3D scanning's use in other studies conducted in more traditional environments, such as bridge structures; while not as extreme, access is still a pressing challenge that can be eased using 3D scanning technologies.

While many of the above studies focused on the applicability of photogrammetry in infrastructure monitoring, there has been significant research conducted with LiDAR technology for infrastructure deterioration monitoring and investigation. Additionally, the above studies primarily focused on deflections of global structures and structural members, while Chen and Liu have investigated damage and defect detection but have done so by means of LiDAR technology *(43, 44, 45)*. Chen and Liu primarily investigated structural health monitoring in the form of crack detection and concrete defect or mass loss, respectfully *(43, 44, 45)*. Liu had a heavy focus on bridge health monitoring (BHM) through the lens of terrestrial LiDAR data and defect mapping for bridge rating *(44,45)*. Through a case study on a concrete girder bridge, Liu tested LiDAR scanning on an existing bridge structure and created a proposed method for bridge rating concrete girders based on this study, which can "detect relatively large defect on flat surfaces" *(44, 45)*. Liu also highlights the major potential that LiDAR has in improving the field of bridge inspection due to its repeatability and the speed if paired with an automated data processing method *(44, 45)*. Chen conducted a series of case studies that spanned concrete mass losses in bridge structures, damage quantification, and crack detection *(43)*. The key tradeoffs that Chen discusses as a result of using LiDAR scanning for the means of the case studies are the limitations between speed of scanning and resulting detail and accuracy; how if higher detail is required or desired, the resulting scan time will increase to ensure higher density of points *(43)*. Additionally, Chen highlights two key advantages that are a common theme among scanning in infrastructure and particularly for bridge structures: that there is limited or no

interference in traffic and how scanning provides a permanent snapshot or record of the structure or component at the time of scanning *(43)*. Overall, many of the studies on LiDAR and photogrammetry for applications in infrastructure deterioration suggested that the speed and amount of data gathered gives the use of the 3D scanning technologies tremendous potential in the areas of bridge inspection and structural monitoring.

From studies in the late 1980s and early 1990s from Bales and Cooper to studies in the early 2010s from Chen and Liu, it has been shown that photogrammetry and LiDAR scanning can provide a historical record and a structural monitoring record for the structure being documented *(39, 40, 43, 44, 45)*. This continues to be an ongoing discussion among many researchers investigating 3D scanning for use in the global structure of deteriorating bridges and infrastructure and also in the localized components.

## 2.8 Member-Based Inspection of Corroded Steel Girders

There have been recent important research studies in corroded beam end capacity estimation specifically. The studies of deteriorated beam ends conducted by Tzortzinis and Javier spanned beams of several sizes with a large spectrum of damage variation and severity *(46-54)*. Javier's specimens were beams varying in size from 8-inch-deep beams to 21-inch-deep, beams while Tzortzinis studied corroded ends where the sections were 21 inches deep and 33 inches deep *(46-54)*. Tzortzinis's experiments and subsequent analysis resulted in creating revised equations for estimating the remaining capacity in a corroded steel beam end *(46-52)*.

Javier directly compared several methods for analyzing and estimating the remaining capacity of corroded beam ends and found that Tzortzinis's performed better than other previous methods of estimating corroded beam end capacity *(46-54)*. Because this remaining capacity directly pertains to the resulting section loss on the web of the beam end, it is critical to be able to estimate this section loss accurately. It was found through the studies conducted by Tzortzinis that the most critical section of the beam end where corrosion-induced section loss is critical to the governing resulting capacity is in the bottom four inches of the web *(46-52)*. Tzortzinis found this through extensive laboratory testing, parametric analysis, and finite element modelling *(46-52)*. Many of these experimental tests and findings were summarized by Tzortzinis in a technical report for MassDOT *(46-52)*. Ultimately, the final version of the capacity estimation equations for corroded steel girders with and without stiffeners and the guidance for corroded web measurements to be performed in the bottom four inches of the web is summarized in the newest edition of the MassDOT Bridge Manual *(55)*. Additionally, the length of this critical area is dependent on beam geometry and on out-of-plane web deviation, a parameter found and introduced by Tzortzinis *(46-52)*. The graphic of the area of interest on the corroded web for capacity estimation taken from the MassDOT Bridge Manual is found in Figure 2.7 below *(55)*.

Alongside the multitude of assessments performed on corroded beam ends, there has been

significant prior research conducted using both LiDAR and photogrammetry to generate section loss data on a corroded beam web. Many of these studies were performed as proof of concept in using LiDAR and photogrammetry for bridge inspection of these deteriorated structural members. The studies by Hain et al. discuss using 3D scanning via the Artec Eva photogrammetric scanner *(56)*. The scanner itself is a handheld structure-from-motion scanner that requires a wired laptop connection for use. It is a scanner that constantly captures data of the surface being scanned by stitching several frames together. The researchers of this study were able to capture corroded beam end geometries and section loss in the field and in the lab setting through extensive trial scans. The key findings and contributions of this research were the use of 3D scanning to create 3D models of corroded ends with section loss with some supplemental color maps of section loss. Like other researchers above using photogrammetry, Hain discusses the importance of registration objects and overlaps within the scanning of the desired object or member *(56)*. In two-sided scan scenarios, it is imperative that proper registration and alignment is attained; Hain considers the use of a reference bar of known geometry for alignment and validation purposes *(56)*. With the use of the Artec Eva, an onsite computer was needed, which can be difficult regarding space and access within certain structures and for specific structural members *(56)*. A key theme that is discussed throughout much of the literature is also discussed by Hain: how the contributions of scanning and combining multiple scanning methods can afford the opportunity to recreate entire structures *(56)*. While this was not necessarily the main goal of the work, it is a key observation that has been in discussion among researchers as scanning technologies, methods, and processing abilities continually improve.

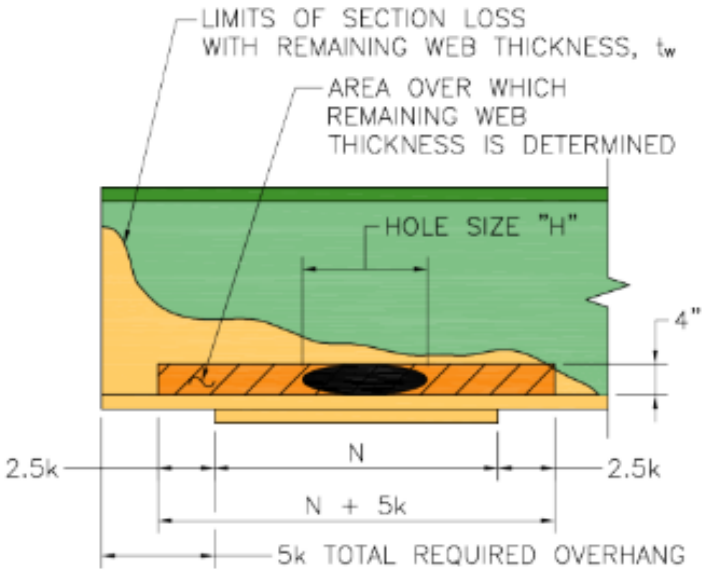


From MassDOT Bridge Manual *(55)*

**Figure 2.7: Corroded web region of interest for capacity estimation**

This is an example of the critical measurement region for corrosion presented by MassDOT *(55)*. It is important to note that the region is 4 inches high and the length of this region is dependent on beam geometry via the parameter "k" in this figure.

Both Hain and Javier used color mapping to describe section loss within the steel girder *(56, 53, 54)*. Hain overlaid or visualized this colormap on the 3D models created using the Artec Eva scanner *(56)*. Example heatmap outputs from Hain are found in Figure 2.8 below *(56)*. While Hain used a handheld photogrammetric scanner and overlaid these heatmaps in the 3D model space, Javier had an alternate approach through generating heatmaps via the data collected with the use of an ARAMIS DIC system *(56,53,54)*. The points that were ultimately used to create the resulting section loss profile in the form of the heat maps were sampled at each half-inch for the shallower beams (S8×18.4 and W10×26 beams) and at each one-inch for the deeper beams (W16×45 and W21×62 beams) due to software constraints *(53,54)*.

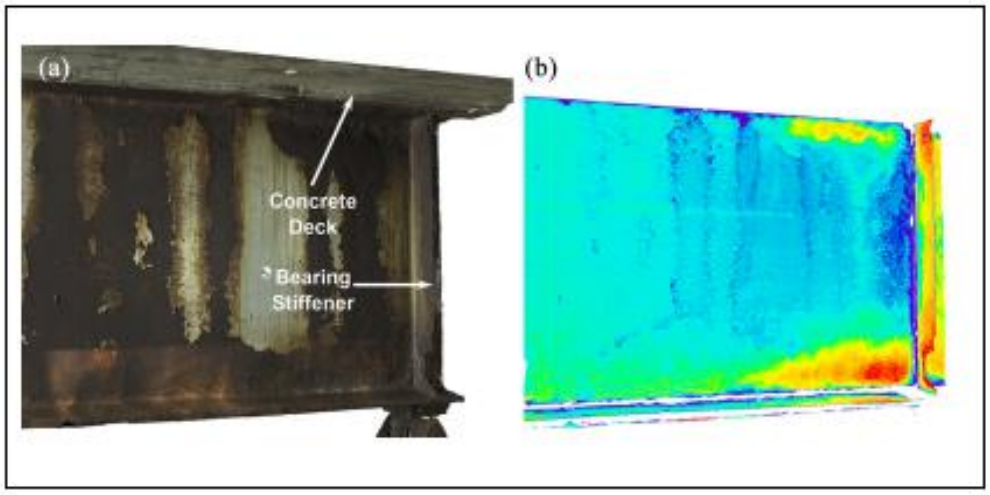


(a) texture (b) coloring mapping to illustrate remaining thickness

From Hain *(56)*

**Figure 2.8: 3-D model of beam end**

Example heatmaps that span multiple beam specimens and varying severity of corrosion damage from Javier are found in Figure 2.9 *(53,54)*. The scanned beam surface with texture and the resulting color mapping were from the use of the Artec Eva photogrammetric scanner. The color mapping for severity is much like that of Javier, where the red in the map in part B of the above figure describes the area of the most severe corrosion-induced section loss exhibited on the beam end and the stiffener *(53, 54, 56)*.

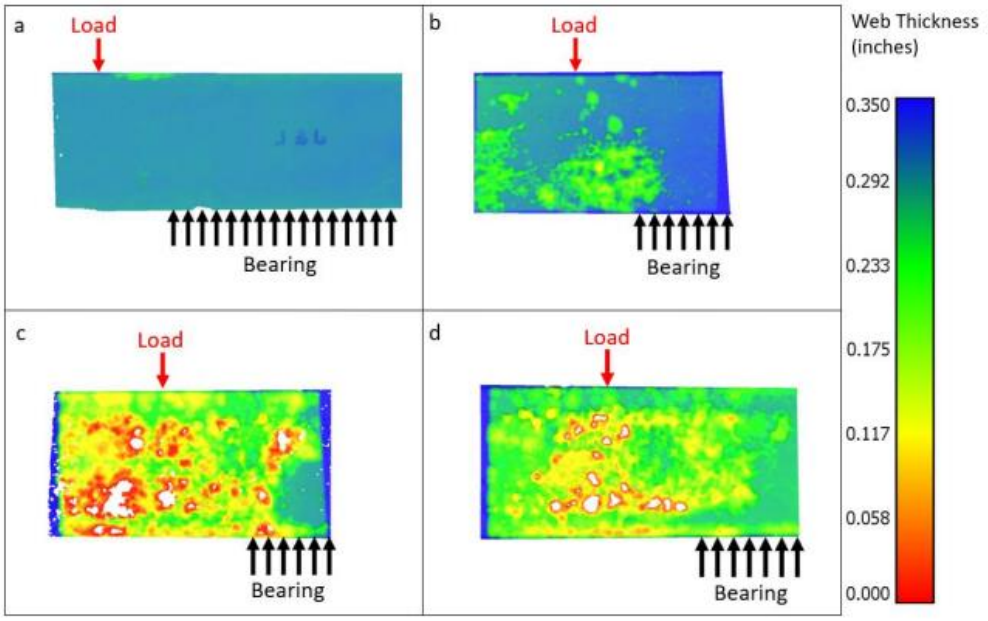


(a)1-S8-L; (b) 2-S8-ML; (c) 3-S8-MH; (d) 4-S8-H

From Javier *(53,54)*

**Figure 2.9: Heat maps showing web thickness of S8×18.4 beam end specimens**

The figure illustrates Javier's use of corrosion heat maps from scanning output using the ARAMIS DIC system *(53,54)*. The blue color in the above figure represents intact or nearly intact web thickness while the red represents the areas of the most significant section loss due to corrosion. It is also important to note the areas of total section loss, or corrosion-induced holes, which are depicted in white *(53,54)*.

While many researchers have focused on the remaining thickness of a corroded end, there are instances of severe damage in the form of areas of entire section loss or corrosion-induced holes, which is commonly observed on the structural members. Remaining thickness of the damaged steel is imperative to calculate for the remaining capacity, and the severity of corrosion-induced holes directly reduce the capacity and capacity estimations for a beam end. Using laser scanning, Truong-Hong et al. captured point clouds and employed methods of point-cloud analysis to identify and measure hole dimensions, such as area, within corroded beam ends specifically *(22,57)*. A simplified depiction of Truong-Hong's process and method for areas of entire web section loss is found in Figure 2.10 *(57)*.

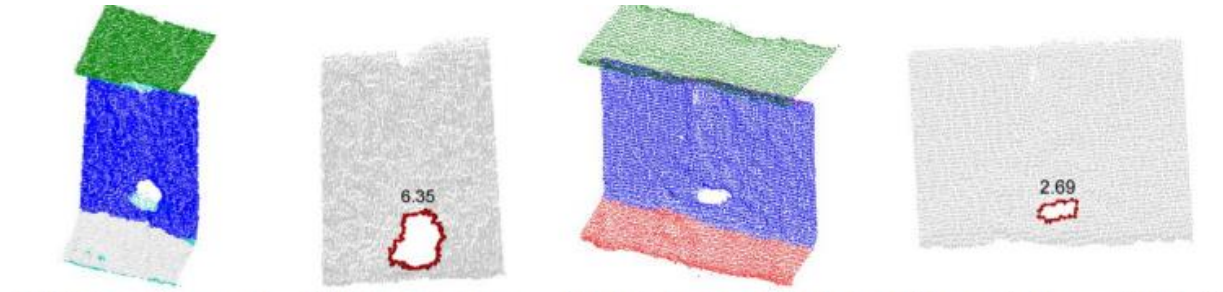


From Truong-Hong et al. *(57)*

**Figure 2.10: Proposed method of determining areas of surface loss of Beam No. 3 (unit in $cm^2$)**

The figure demonstrates the process for computing areas of holes for a corroded steel beam end proposed by Truong-Hong using point-cloud data *(57)*.

Tzortzinis et al., Gerasimidis et al., and Casas present a processing methodology and several tests on real corroded beam specimens using conventional methods, such as the use of an ultrasonic thickness gauge, and LiDAR 3D scanning technologies to document corroded beam end section loss *(58-65)*. Tzortzinis et al. used the Reigl VZ-2000 for the scanning of the corroded ends and did so via scanning both sides of the beam end and manually aligning them via point picking *(58-63)*. Tzortzinis et al. created a flowchart and methodology of processing point-cloud data for corroded beam ends via LiDAR point clouds *(59,60,62,63)*. The point-cloud processing methodology presented by Tzortzinis had the main goals of thickness estimation, analytical capacity estimation, and computational capacity estimation, which are found in Figure 2.11 *(60,62)*.

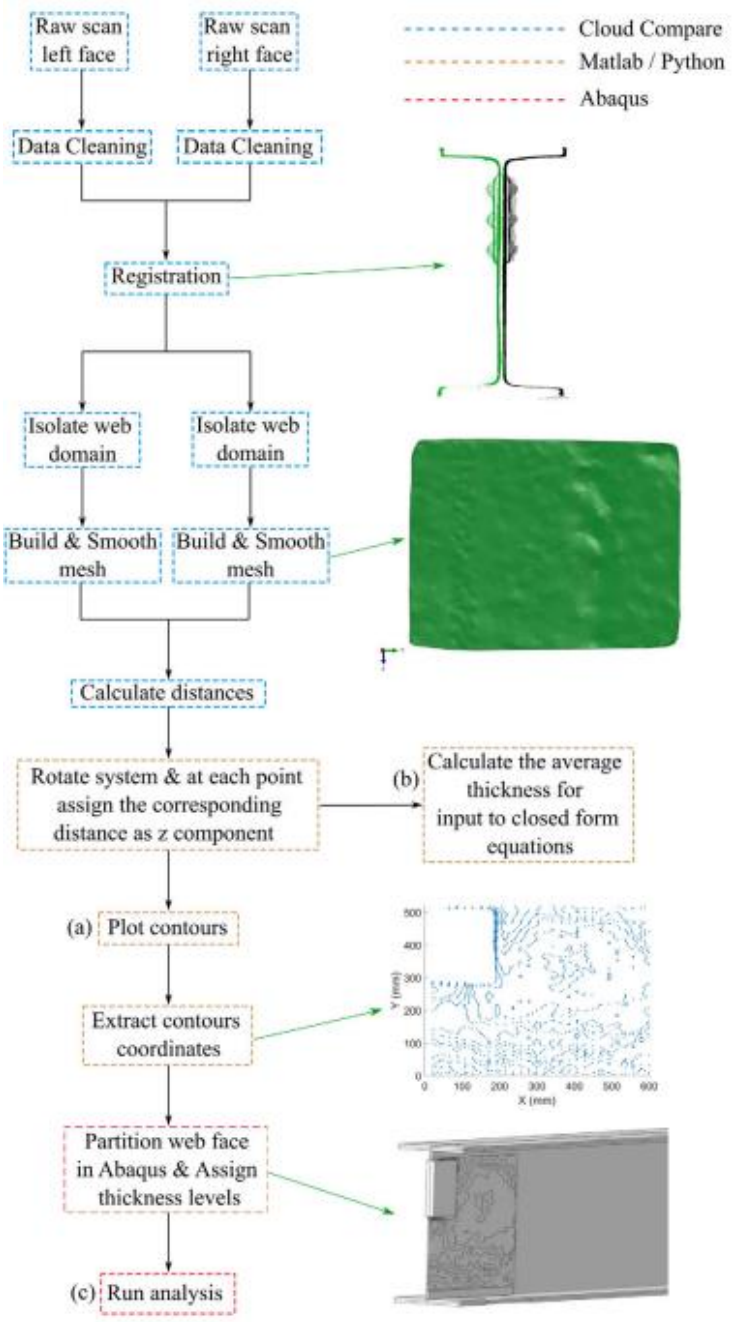


(a) thickness estimation, (b) analytical, and (c) computational capacity assessment.
From Tzortzinis *(60)*.

**Figure 2.11: Point cloud data processing methodology**

The figure shows the process created by Tzortzinis for capturing point-cloud data from a corroded beam end *(60)*. This includes a thickness estimation that is made between the two

scanned surfaces of the web, the analytical capacity estimation via the average remaining thickness found and the beam geometry, and the computational capacity estimation through importing the resulting thickness contour into a finite element software *(60)*.

The methods developed by Tzortzinis were ultimately used as the method for the documentation of stiffened corroded beam ends, a protocol developed for inspection and assessment, and selected specimens in the work on convolutional neural networks for capacity estimation in 2023 *(59-63)*. Much like the previous researchers who documented corroded girders via scanning, Kanakamedala used contour maps to describe corrosion-induced section loss on bridge girders *(65)*. The section loss observed was natural on selected girders and artificially increased in other girder specimens. The bridge girder corroded webs were documented by traditional means, like the use of an ultrasonic thickness gauge. Additionally, Kanakamedala and their research team used photogrammetry via a custom rig, eight cameras, and a path around the beam specimen *(65)*. The path of their documentation process can be found in part (a) of Figure 2.12. They used the point-cloud data extracted to create 3D models of the specimen and to extract the profiles of section loss exhibited on the corroded beam specimens and directly compare the section loss profile to the measurements recorded from the ultrasonic thickness gauge *(65)*. The resulting profiles were also used to create a detailed finite element analysis model *(65)*.

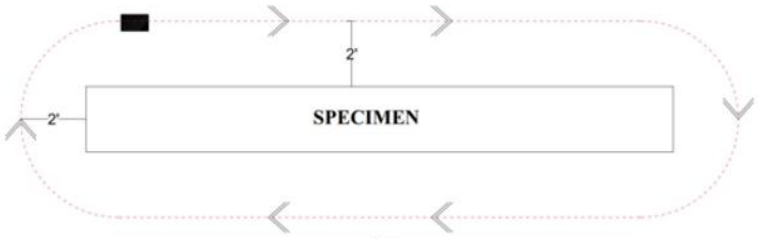


(a)

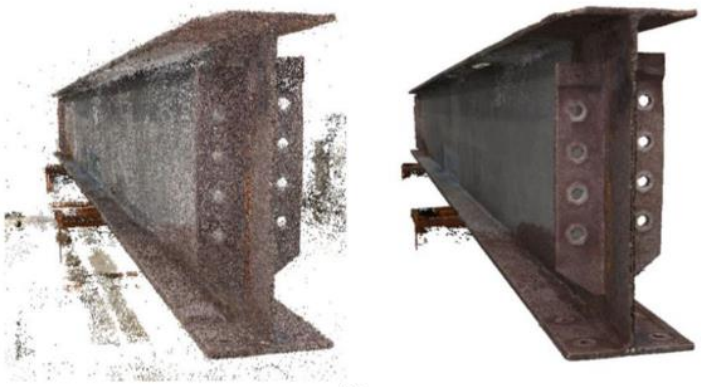

(b)

(a)Path traversed around the specimen (plan view) (b)Comparison of tie-point cloud and dense point cloud From Kanakamedala *(65)*

**Figure 2.12: Example of photogrammetry used by Kanakamedala et.al.**

The variety of scanning methods and technologies raises the discussion of acceptable accuracy and the idea of scale. In the previous sections, many researchers employed drones and other types of UAVs to assist in the infrastructure monitoring and damage detection process. Additionally, various LiDAR units have been introduced with varying ranges and accuracies. In all the above studies, it is important to remember the scale of the measurement being taken and accuracy of the equipment being used. For example, a user of LiDAR or photogrammetry in visual inspection or in the creation of a digital twin of a large structure may aim for an acceptable error on the centimeter scale, where a user of LiDAR or photogrammetry for steel section loss in a corroded beam may aim for an allowable error on the sub-millimeter scale. Each piece of scanning equipment, each scanning environment, and the scale of each object being scanned will introduce sources of error to the resulting data outputs.

While scanning has been proven to be an accurate and precise way of measuring deterioration and section loss of steel girders specifically, there are key errors that can take place in the scanning process that users need to be aware of. Bian et al. discuss these errors across the entire process for bridge inspection: spanning errors during data collection, data analysis and processing, and environmental factors *(66)*. On a global bridge inspection scale, Bian et al. found that scanning angle variance and "damage evaluation algorithms" were the main sources of error *(66)*. On the other hand, for member inspection, these challenges become different; in the work of Tzortzinis, misalignment of LiDAR point-cloud scans was a challenge and possible source of error, while Hain discusses the error generated with high reflectivity objects for structured-light photogrammetric scanners *(58-63,56)*.

This page left blank intentionally.

# 3.0 Research Methodology and Protocol

The following chapter discusses the research methodology and protocol created by the research team for scanning corroded beam ends using two different types of 3D scanners. The two scanning technologies used within this study were LiDAR and photogrammetry. The full and summarized version of the scanning protocol proposed and developed by the University of Massachusetts research team can be found in the Implementation and Technology Transfer section of this report.

## 3.1 Point Measurement

For Laboratory Beams 1 and 2, thickness grids were created to take evenly spaced point measurements of the web thickness to create a grid that would represent the thickness profile of the corroded beam web. Additionally, these point measurements were used as a means to check or validate the data taken from the 3D scanners. The tool that was used by the research team for these point measurements was the GE PocketMIKE, which is an ultrasonic thickness gauge that is used, or is an equivalent, to a hand tool used by bridge inspectors to measure web thickness *(67)*. The PocketMIKE was tested against a steel block of known thickness to test the performance of the tool while measurements were taken in the laboratory and field setting *(67)*. These thickness grids were only generated in the laboratory as time and accessibility limited this from being used in the field. While this is the case, several point measurements were taken in the field-scanning task of this project. Representative thickness grids from Laboratory Specimens 1 and 2 are found in Figure 3.1 below.

**Figure 3.1: Point measurement grids for PocketMIKE *(67)* ultrasonic thickness gauge**

## 3.2 Scanning Machinery

This research study considered two types of 3D scanners: the Riegl VZ-2000 and the Artec LEO *(69, 70)*.

The Riegl VZ-2000 is a time-of-flight terrestrial scanner that uses Light Detection and Ranging, or LiDAR, to generate point clouds of the surfaces it scans *(69)*. This machine remains in a static position during operation. With its wide range and field of view, the Riegl can capture data for objects or locations that are very large in size. This allows for many points to be captured that will overlap among scans, which is a critical part of the current study. For sufficient alignment, four or more pairs of points shared between two scans must be found and selected manually via point cloud computing software. The research team used CloudCompare, an open-source software for point-cloud operations, for this manual alignment *(68)*.

The Artec LEO is a handheld structure-from-motion (SfM) scanner that is based in photogrammetry, where photos are constantly stitched together to form an object or surface. Its handheld nature and need to be moved to perform the scan make it easy to capture the surfaces that a user wants scanned. The Artec LEO has an accompanying software in which registration and alignment can take place. While there are cases where Artec Studio provides sufficient alignment via its semiautomated and artificial intelligence-driven processes, further rigorous alignment may be necessary via manual point picking in CloudCompare or the Iterative Closest Point (ICP) method depending on the size and quality of the scan performed *(68)*. Alignment methods are further discussed in the section titled Registration and Alignment, and more detailed specifications for the Riegl VZ-2000 and Artec LEO scanners can be found in the Implementation and Technology Transfer section of this report as well as through their respective manuals *(69,70)*.

## 3.3 Path Planning Details

During laboratory scans, it is straightforward to plan the path of scanning as well as place registration points for point-cloud processing following the scans. Beams for laboratory scanning are typically performed one at a time as they are no longer a part of the bridge system. When using the Reigl VZ-2000 LiDAR scanner, the research team could place the machine on a cart to scan one side of the beam, then move the system to the other side to complete the second scan *(69)*. The path planning in these cases was ensuring full visibility of the corroded end on both sides with the system arranged as close as possible; the Reigl VZ-2000 has a minimum scanning distance of around 2.5 meters, so objects closer than this would not be recognized *(69)*. When using the Artec LEO in the laboratory setting, the path planning was low-demand as the handheld unit could be used for a two-sided scan to mimic field work or could be performed in a closed-loop manner *(70)*.

For field scanning, trip planning is essential as scanning and inspection in general may warrant the closing of lanes, personnel for flagging or signaling, or other methods that limit traffic and cost money to have in place. Based on field scans conducted by the research team, it is imperative to have the bridge plans and the latest inspection report, which will allow for a planning path to be generated based on the need of the structure. Essentially, marking the members/locations of interest based on need for documentation or inspection becomes less demanding when the layout of the structure and the areas of most need are summarized together. Additionally, as part of the path planning, it is critical to know what equipment will be needed to reach the desired parts of the structure that need to be scanned.

To access the beam ends of interest on a structure, it is typical that they could be reached using a bucket truck/snooper, a ladder, and sometimes by foot. Any and all of these tools can be used, but it is important to plan (as done in current practice) for which areas of the bridge will need each tool, as the larger utilities, like the bucket truck or snooper, will require lane closures. Additionally, proper path planning will allow for one lane closure at a time where multiple beams can be scanned in sequence. Figure 3.2 below shows a bridge plan where all of the beams in the middle span of the bridge required a bucket truck to access. To optimize the scanning path, the research team scanned the beam ends on one side rather than scanning by beam. For example, using the sketch in Figure 3.2, the research team would choose to scan beam ends 6, 9, 10, 12, 15, and 16 in that order so the same lane on the left would remain closed and the MassDOT crew would not have to switch between lane closures. This kind of planning can maximize the beam ends scanned while minimizing time and cost.

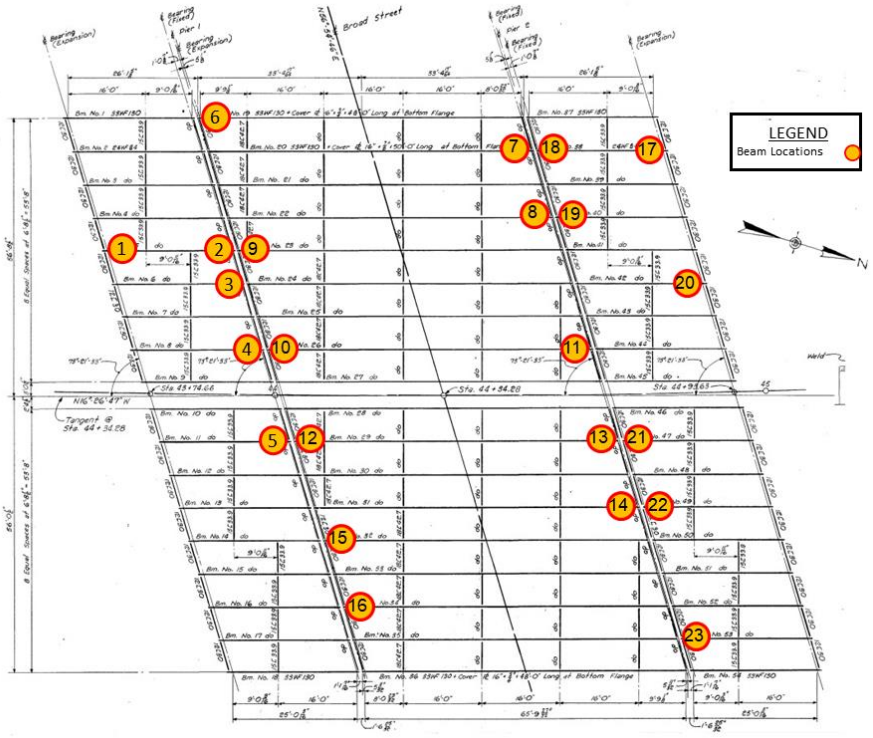


**Figure 3.2. Example scanning plan for a highway bridge**

## 3.4 Scanning Methods

The scanning methods discussed here are implemented into the protocol proposed by the research team in the Implementation and Technology Transfer section of this report. To conduct the scans presented in this report, individual methods had to be performed for the Reigl VZ-2000 and the Artec LEO *(69, 70)*. Following path planning and registration object placement, the actual scanning of the desired object or location must take place. In the case of this research project, the area of interest is the corroded end of the beam. Overall, in the scanning process, it is key to capture all necessary areas of the beam end that need to be documented and it is critical to capture several alignment points or objects within the same scan. Alignment objects must be visible by both scans performed, assuming the scan of the beam is conducted using two-sided scanning. When the Artec LEO is being used for scanning, the surfaces and objects of interest (which include the beam and registration points/objects) can constantly be seen; the Artec LEO is constantly stitching frames of scanned objects/surfaces together to create the final scan *(70)*.

While the scan is being conducted by the user, speed and scanning distance become other crucial components to the overall quality of the resulting scan. SourceGraphics/Artec supply an operating distance of 0.35 to 1.2 meters via their documentation of the Artec LEO scanner *(18,70)*. On board the Artec LEO and stated above, the scan can continuously be analyzed and observed; conveniently, visualization filters can be applied while the scan is taking place, which pertain to scan quality, optimal distance, or other filters of interest *(70)*. For the purposes of this work conducted, the research team used the optimal distance filter. The color of the surface during the recording will tell the user whether the surface being scanned is within the optimal distance or is too close or too far from the object. A yellow to red surface will appear for objects too close to the scanner while a teal to blue surface will appear for objects too far from the scanner. Once an object is entirely out of range in either of these directions, it will disappear and not be recorded by the scanner. The optimal or "good" scanning distance provided by SourceGraphics/Artec is in the range of 0.45 to 0.85 meters and will appear in green. Similarly for the scan quality filter, a "well scanned" area will be denoted in green while yellow to orange is described as a "sufficiently scanned" area and red is denoted as an "insufficiently" scanned area *(70)*. Across these cases, it is imperative to maintain a "good speed" and change the angles of scanning to ensure all parts of the desired surface are captured (which includes pits, holes, or other abnormalities in the scanned surface) and significant amounts of the registration objects are captured. A "good speed" for the Artec LEO based on the work of the research team is a pace slow enough for the beam and other objects to be recorded without causing the scanner to lose track of the object but not so slow as to create too large of a file size *(70)*. This pace will vary depending on the damage in the beam, the beam size, the access to members/structure, and if more angles are necessary to capture the objects of interest. The user, as they scan more frequently, will develop this pace for each of the beam ends they need to scan. Ultimately, while using the Artec LEO, it is not demanding to analyze the quality of the scan being conducted by the user, but the path and pace of the scan being performed will take experience of the user/inspector and will vary on a case-by-case basis *(70)*. This scanning method was used for all of the beam specimens in this report aside from Laboratory Beam 1.

The scanning method used for the Laboratory Beam 1 specimen was a two-sided scan performed with the Reigl VZ-2000 *(69)*. The Reigl VZ-2000 was placed to scan the corroded beam end at approximately a 90-degree angle, or perpendicular to the beam web *(69)*. This was done primarily to record the most data points on the corroded end as the Reigl VZ-2000 records data points at prescribed intervals and will move/rotate to scan at a prescribed pace but was also placed to ensure the capture of alignment points *(69)*. As the alignment had to be performed with manual point picking, the team used the checkerboard registration objects discussed in the next section, Registration and Alignment. As the Reigl VZ-2000 provides significant amounts of data in the form of a point cloud, its large size makes it difficult for bridge inspectors to carry up to a corroded beam end *(69)*. While this is the case, the research team was still able to use the Reigl in a laboratory environment.

While undergoing both laboratory and field scans and with thorough discussions with the research team and through conversations and guidelines provided by SourceGraphics and Artec 3D, the team found that there were certain situations, objects, or areas to avoid during scanning that could cause error or unsuccessful scanning. The most critical objects or areas to avoid were overly shiny or reflective objects, areas with significant uniformity in color, transparent/translucent objects, and wet areas. The scanning protocol developed and documented in the Implementation and Technology Transfer section of this report is catered to the Artec LEO handheld scanner, which the research team used for all but the Laboratory Beam 1 specimen *(70)*.

## 3.5 Registration and Alignment

Alignment and registration are two critical components of the scanning process, as misalignment and errors in registration can cause inaccuracies in the final contour maps and heat maps, and thus the thickness measurements taken from the scanning. While there will always be error due to factors such as scanning conditions (e.g., weather, accessibility) or small misalignments, it is imperative to register the scans as best as possible. To avoid alignment error, environments where the scan of an entire beam end (both sides) can be captured in a single pass via a closed loop scan would be the most advantageous. Closed-loop scans can typically be conducted where an inspector can easily access the beam end by foot and walk or duck under the beam to reach both sides. While there are some environments or situations like this where accessibility allows a closed-loop scan, many or the majority of scans will have to be performed in a two-sided manner.

For two-sided scans, the research team considered three routes for alignment and registration which depend upon the scanner used and what is contained in the scan itself. While using the Riegl VZ-2000, the research team used manual point picking, where shared points in two scans are chosen to align the two sides *(69)*. Typically, four to six points were chosen to align the scans as too few points would not create a sufficient alignment and too many could create error through over-registration or "overfitting" *(28, 29,30)*. While using the Artec LEO, the researchers used the built-in tools of the Artec Studio Software; these tools included point

picking in some cases with additional features that include alignment via texture and colorization through the artificial intelligence-driven auto-alignment and global registration *(70, 72)*. Finally, the Iterative Closest Point (ICP) method was used as the alignment method for a two-sided scan. For the field scans in particular, some scans faced alignment difficulties using the point picking method listed above; it was not sufficient in aligning the two sides of the beam end scans so the ICP algorithm shown in Table 3.1 was used to attain an adequate alignment.

**Table 3.1: Algorithm for iterative closest point (ICP) for beam scans**

| Iterative closest point algorithm |
|---|
| Require: $S$: Point cloud data from Scan 1<br>$D$: Point cloud data from Scan 2<br>Ensure: $T$: Transformation matrix<br>1: $T \leftarrow I$<br>2: while $notconverged$ do<br>3: for $di \in D$ do<br>4: $ki \leftarrow find\ closest\ points(S, di\ , T)$<br>5: end for<br>6: $T \leftarrow argmin$ Íi $\|ki - T \cdot di\ \|2$<br>7: end while<br>8: return $T$ |

Registration objects were used to align the two sides of the scans in the laboratory environment and for the field scans. For the Riegl VZ-2000 scanner, checkerboard patterns were used around the beam specimen within the lab *(69)*. The Riegl can read reflectance intensity, making checkerboards perfect for point registration for both their sharp corners and also their stark differences in reflectance via the black and white colors. For scans with the Artec LEO, the team investigated matte red plastic L-shaped beams *(70)*. These beams were cut and magnets were glued onto them for versatility, allowing them to be placed on the pier, the beam, or other metal objects surrounding the beam end of interest. Additionally, sticker lettering was placed on these red beams to allow for sharp corners and distinctive coloration. Like the Riegl VZ-2000 scans, square checkerboard pattern pieces were placed on or around the beam to act as additional point and coloration objects for registration. Finally, registration spheres were explored for use in the scanning process. These SECO spheres were matte white, made of aluminum, and attached to a magnet base *(73)*. These, like the red beams, were chosen for versatility in placement of the object, the stand allowing the sphere to be placed on the pier and the magnet allowing the sphere to be placed anywhere on the beam or surrounding metal objects. The sphere shape allowed for an easy recognition in shape as well as a multifaceted object, which allows for a better alignment between scans. For the field scans in particular, it was critical to capture parts of the pier or abutment below the beam end as this surface creates a great surface to be used for auto-alignment via Artec Studio and/or for the use of the ICP algorithm to visibly see sufficient surface overlap between the two scans *(72)*.

These registration objects and surfaces were beneficial in the point registration and auto-alignment process as the Artec Studio software recognizes coloration and texture *(72)*. It is imperative that these registration objects varied in orientation throughout the XYZ axes as having objects very close together can lead to bias in the alignment and ultimately error in the desired web thickness results. Capturing these objects in both scans was critical as they would be used to align the two sides of the scans. If alignment with the registration points or auto-alignment was not sufficient or possible, the ICP alignment algorithm was used to align the scans.

This page left blank intentionally.

# 4.0 Laboratory and Field Results

The following chapter includes a total of eight scans performed as a part of this project. Four of these scans were performed as a part of the laboratory test scans at the Brack structural engineering laboratory at the University of Massachusetts–Amherst. The other four scans were completed as the field application portion of this project, which was conducted on an in-service highway bridge in Springfield, Massachusetts. The four beams scanned for the laboratory scanning task of this work were selected based on their corrosion damage and variation in corrosion profiles. The four beams scanned in the field application phase were some of the beams with the most damage present on the structure and were also chosen due to their variance in profiles. All of the remaining thickness contour maps were generated in the commercial coding software MATLAB *(71)*.

## 4.1 Laboratory Beam Specimens

### 4.1.1 Laboratory Beam 1

Laboratory Beam 1 came from the 02929 bridge on Route 80 in Deep River, Connecticut, but originally came from another structure of unknown origin as a rehab member. Per laboratory measurements and structural drawings, a 20″ deep American Standard was assumed to be the shape of the structural member. The Riegl VZ-2000 was used to document the section loss present on the beam end *(69)*. While it exhibited a common corrosion pattern of full height section loss, the area of most critical section loss can be observed at the mid-height of the web in this specimen.

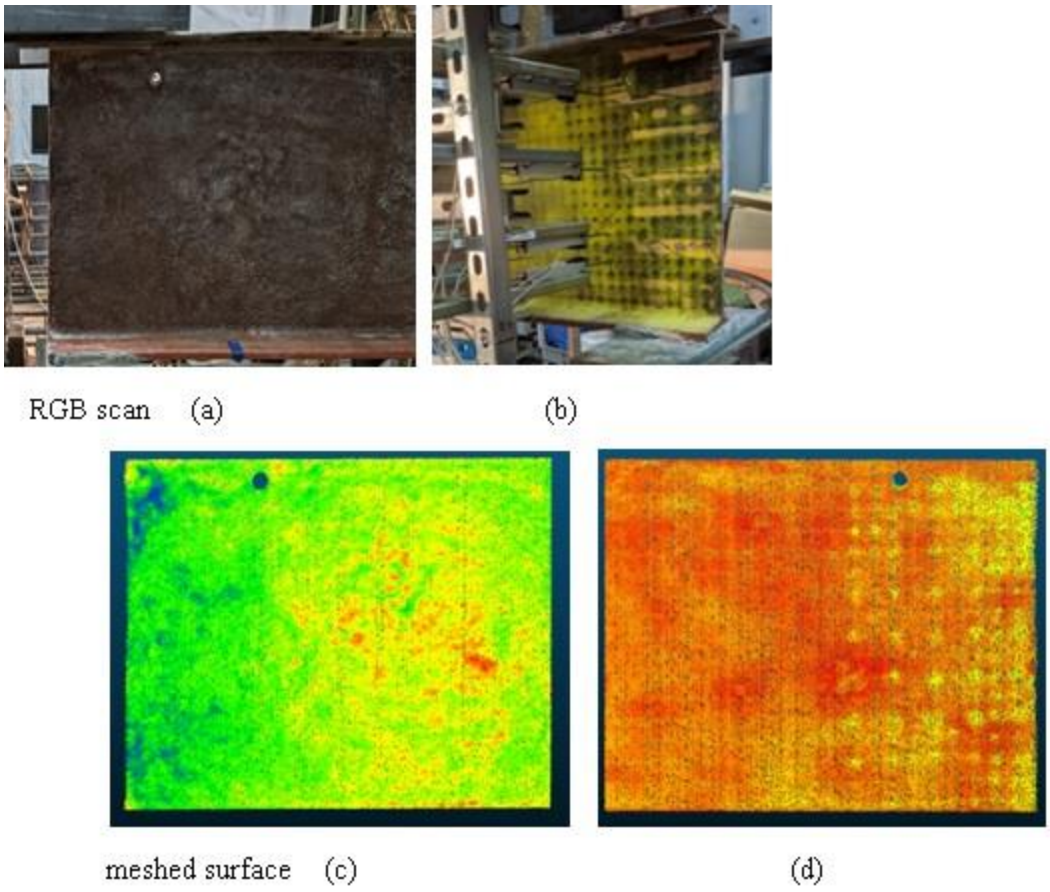


**Figure 4.1: Laboratory beam 1**

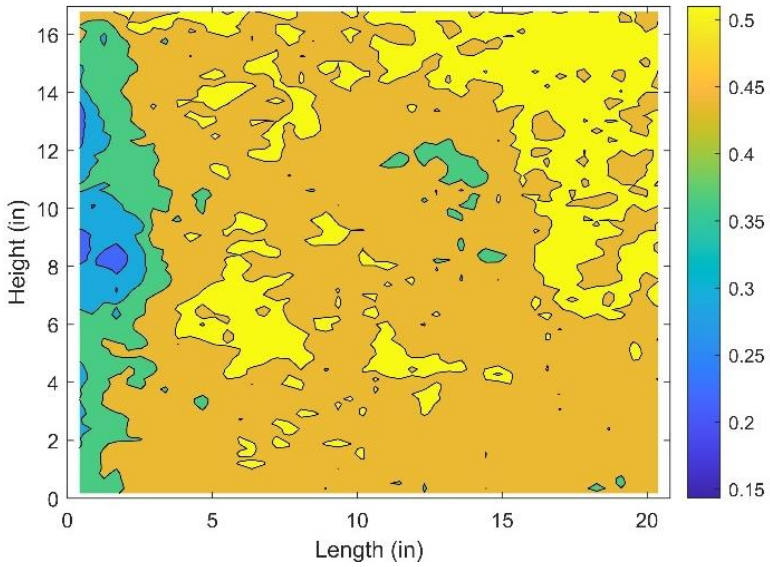


**Figure 4.2: Laboratory beam 1 contour map of remaining thickness**

The contour map in Figure 4.2 shows the remaining thickness of intact steel in the web of the beam, where the darker blue represents the thinnest steel and the yellow represents the nominal, or original, thickness of the web.

### 4.1.2 Laboratory Beam 2

Laboratory Beam 2 came from the 3801 bridge in Jay, Maine. Per laboratory measurements and structural drawings, a B33×132 was assumed to be the shape of the structural member. The Artec Leo handheld scanner was used to document the beam end's corrosion. The area of most critical section loss can be observed at the very top of the web in this specimen, and moderate section loss was present at the base of the web.

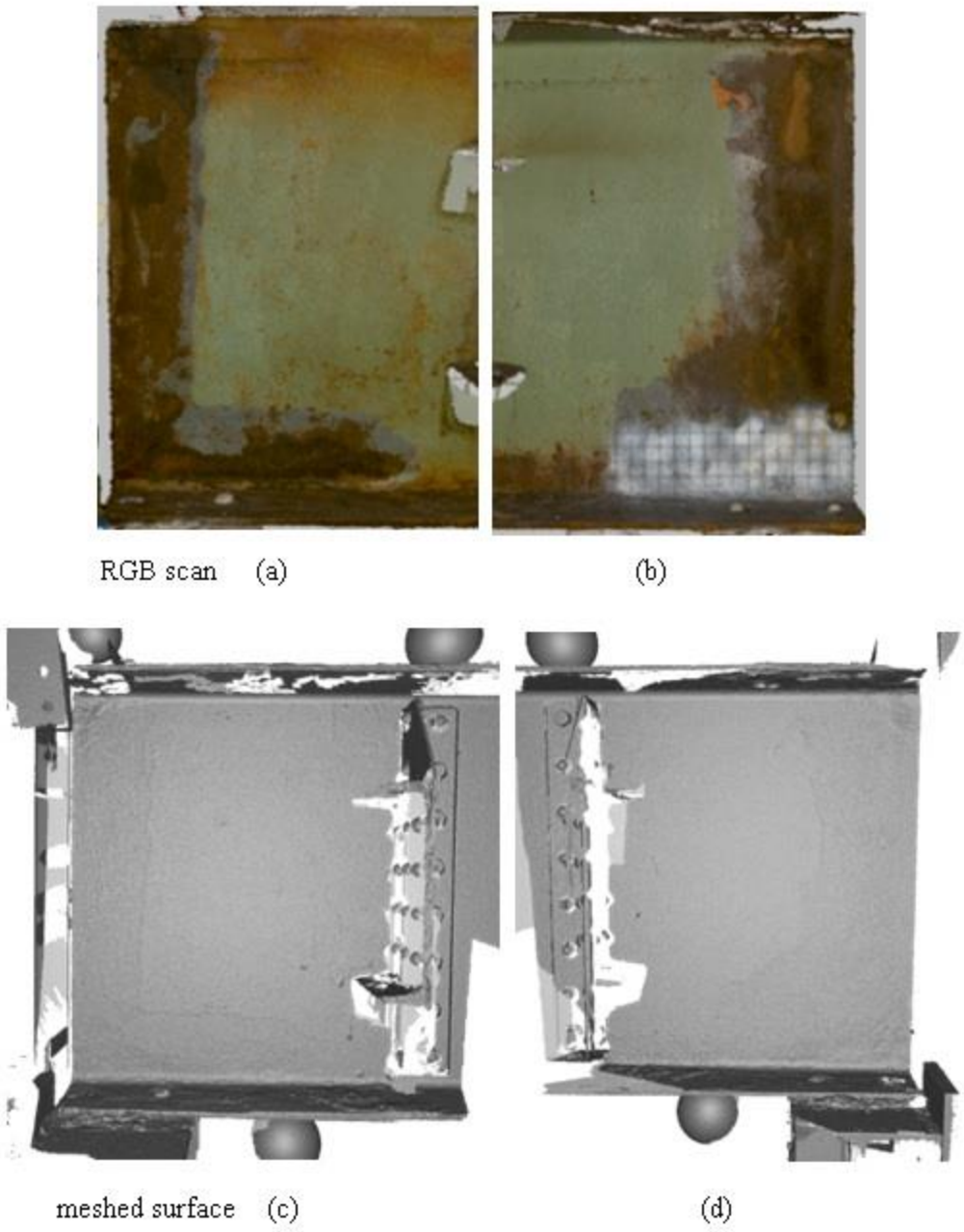


**Figure 4.3: Laboratory beam 2**

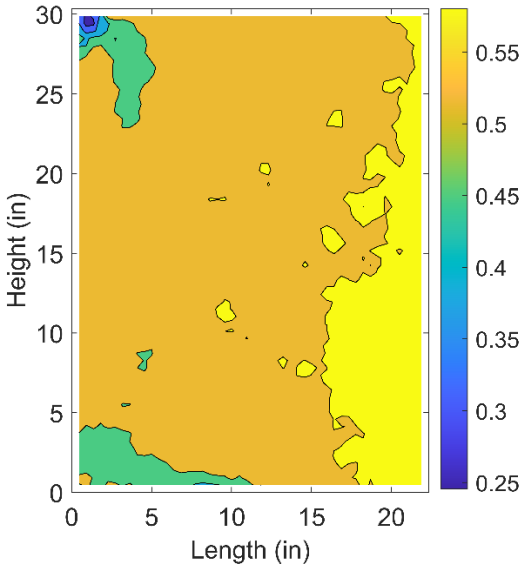


**Figure 4.4. Laboratory beam 2 contour map of remaining thickness**

The contour map in Figure 4.4 above shows the remaining thickness of intact steel in the web of the beam, where the darker blue represents the thinnest steel and the yellow represents the nominal, or original, thickness of the web.

### 4.1.3 Laboratory Beam 3

Laboratory Beam 3 came from the 3801 bridge in Jay, Maine. Per laboratory measurements and structural drawings, a B33×132 was assumed to be the shape of the structural member. The Artec LEO handheld scanner was used to document the beam end's corrosion *(70)*. The area of most critical section loss can be observed at the base of the web in this specimen. A unique property of this specimen was the variation in severity of the corrosion observed on either side of the web; one side of the specimen exhibited little to no corrosion induced section loss while the other side houses most of the section loss.


**Figure 4.5: Laboratory beam 3**

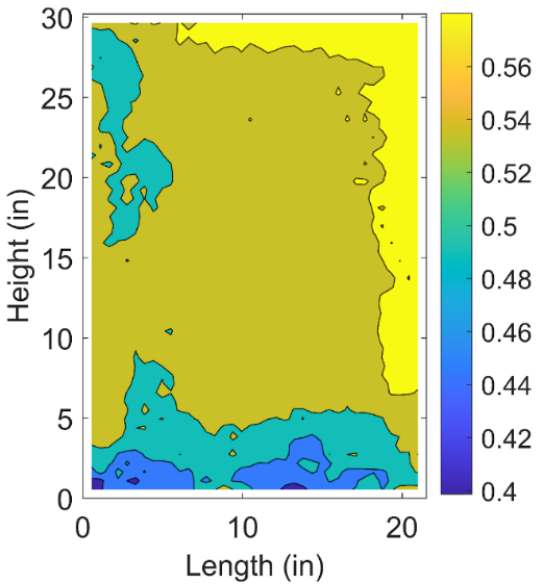


**Figure 4.6: Laboratory beam 3 contour map of remaining thickness**

The contour map in Figure 4.6 above shows the remaining thickness of intact steel in the web of the beam, where the darker blue represents the thinnest steel and the yellow represents the nominal, or original, thickness of the web.

### 4.1.4 Laboratory Beam 4

Laboratory Beam 4 came from the 3801 bridge in Jay, Maine. Per laboratory measurements and structural drawings, a B33×132 was assumed to be the shape of the structural member. The Artec LEO handheld scanner was used to document the beam end's corrosion *(70)*. The area of most critical section loss can be observed at the base of the web in this specimen.

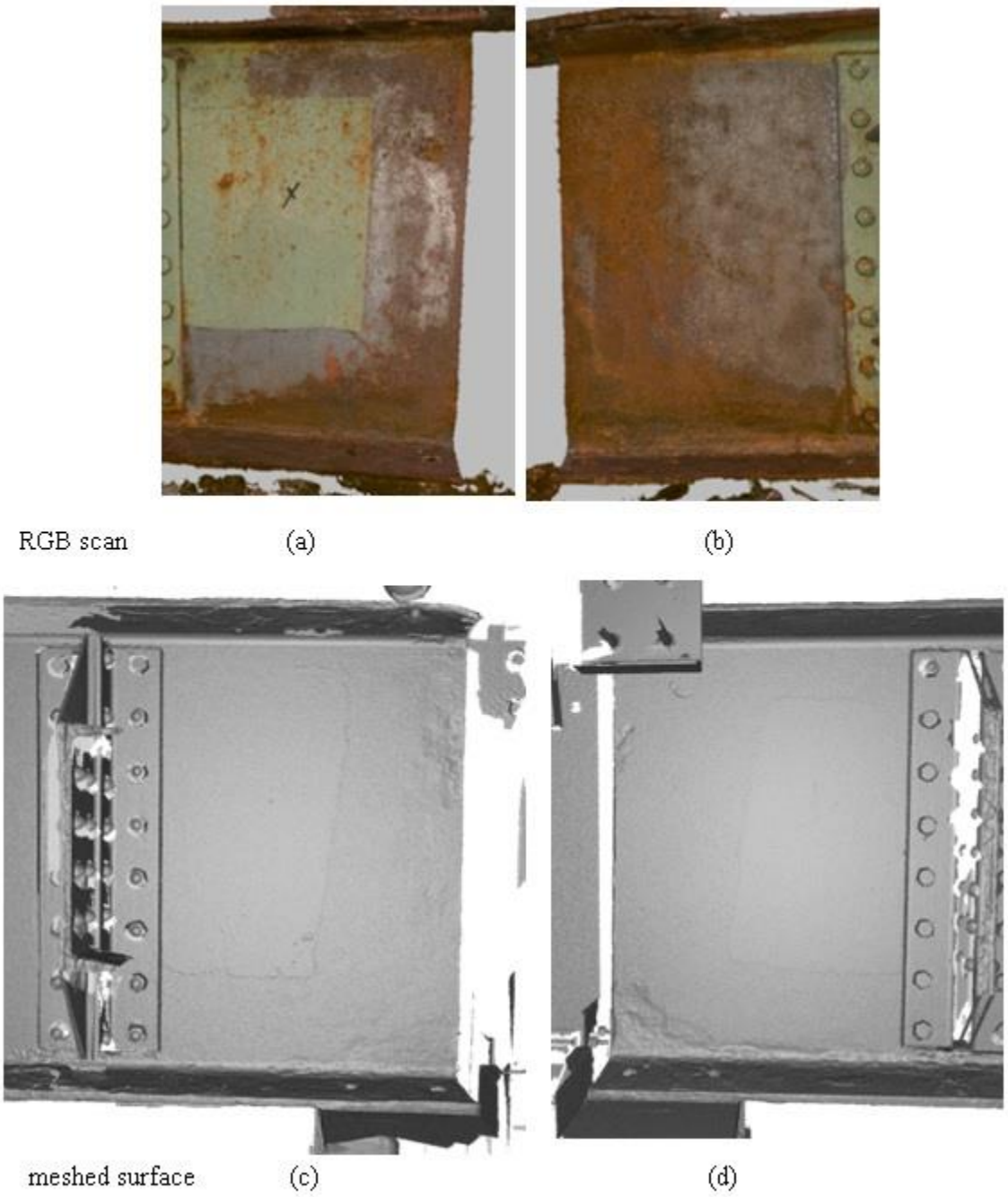


**Figure 4.7: Laboratory beam 4**

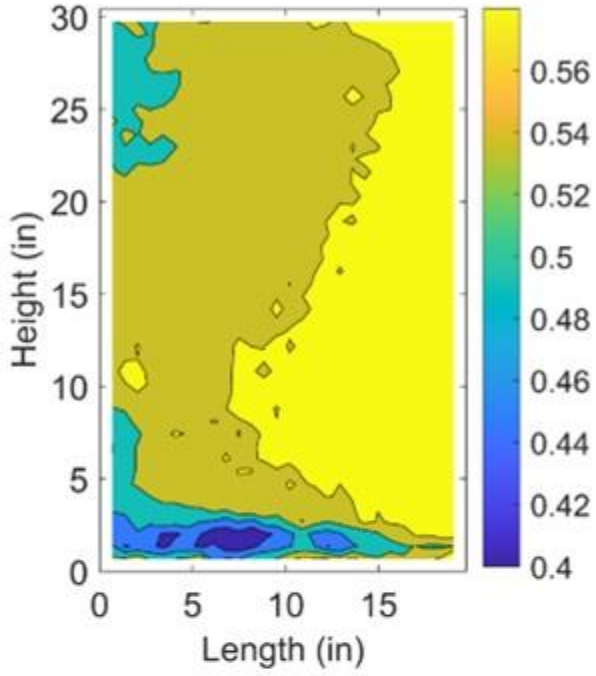


(a) countour map of remianing thickness

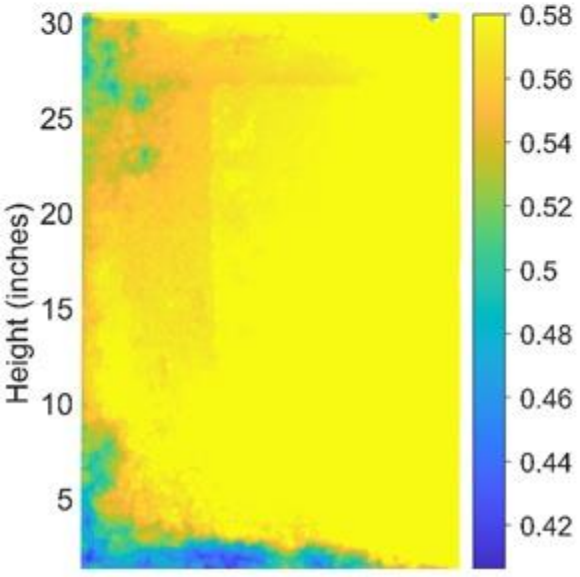


(b) heat map of remaining thickness

**Figure 4.8: Heat and contour map of laboratory beam 4**

The contour map and heat map in Figure 4.8 show the remaining thickness of intact steel in the web of the beam, where the darker blue represents the thinnest steel and the yellow represents the nominal, or original, thickness of the web.

### 4.1.5 Experimental Validation Using Current Inspection Methods and Visual Alignment

For the purposes of this report, the research team employed two ways of validating the 3D scanning data captured. These two methods were by using current inspection tools like the ultrasonic thickness gauge, and through visual checks using textural and geometric alignment methods. Figure 4.9 shows a representative grid of ultrasonic thickness gauge measurements using the PocketMIKE; this grid was designed to take measurements every square inch of the web (1-inch by 1-inch grid) *(67)*. These kinds of grid measurements were taken for the first and second laboratory specimens, where the Reigl VZ-2000 and Artec LEO were used, respectively *(69, 70)*. Lab specimens three and four relied on visual and textural alignment using registration spheres and other overlapping surfaces. Additionally, the alignment of specimens three and four was performed using the auto-alignment features of Artec Studio, which considers similar coloration, texture, and geometry patterns shared by the scans being aligned *(72)*.

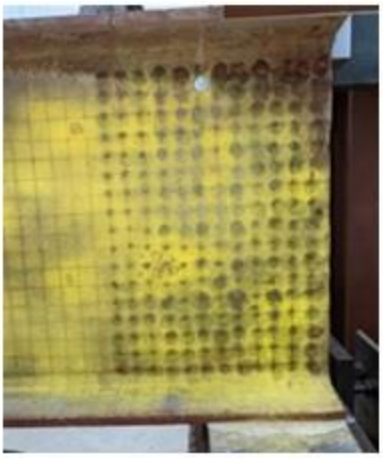

(a) profile of labortory beam 1 from Figure 3.1

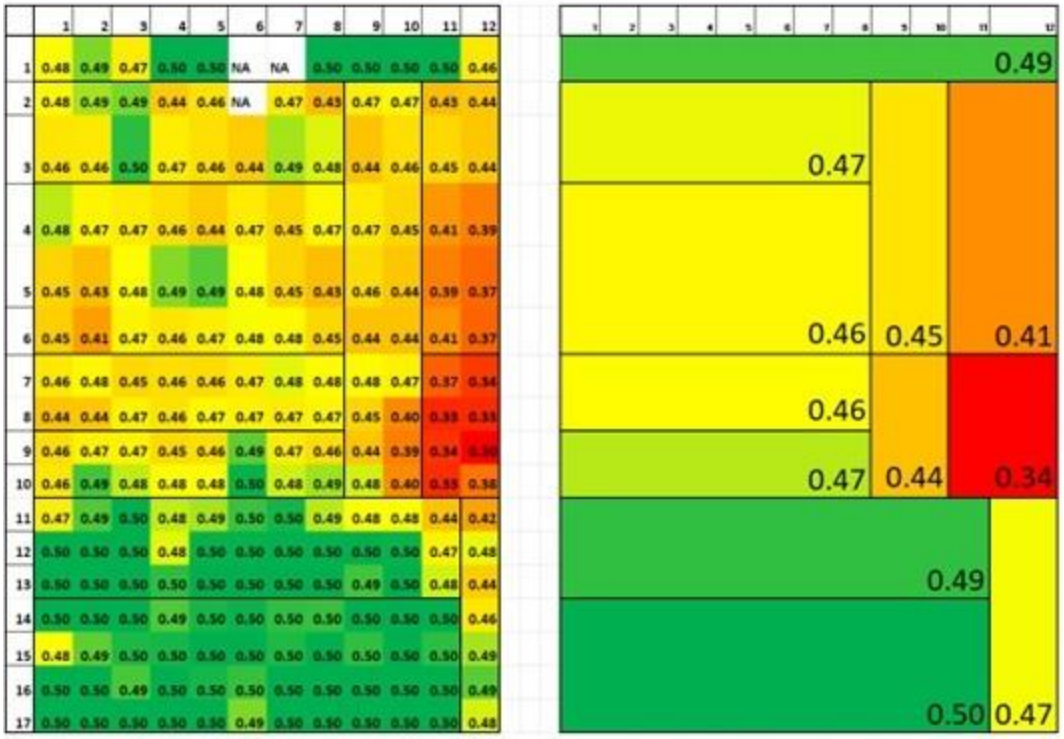


(b) grid of thickness measurements performed by the PocketMIKE *(69)*, lab experiment 1

**Figure 4.9: Profile and thickness measurements of laboratory beam by PocketMIKE *(67)***

Part (b) in Figure 4.9 shows a grid of thickness measurements performed on the corroded beam end in part (a) using the PocketMIKE ultrasonic thickness gauge *(67)*. This process was performed to validate scans by choosing points within this grid to cross-check the corresponding location and its thickness within the resulting profile generated from the scanning process. This was performed rigorously in Laboratory Beam 1 and Laboratory

Beam 2. Throughout the remainder of the experimental specimens, there were other checks performed specifically for alignment and registration of alignment spheres and target points.

## 4.2 Field Beam Specimens

All four field beam specimens were a part of the same interstate bridge in Springfield, Massachusetts. Terrestrial scans of the entire structure were performed by the Reigl VZ-2000 from the ground and on a lift provided and guided by MassDOT personnel *(69)*. The terrestrial scan of the interstate bridge can be found in Figure 4.10.

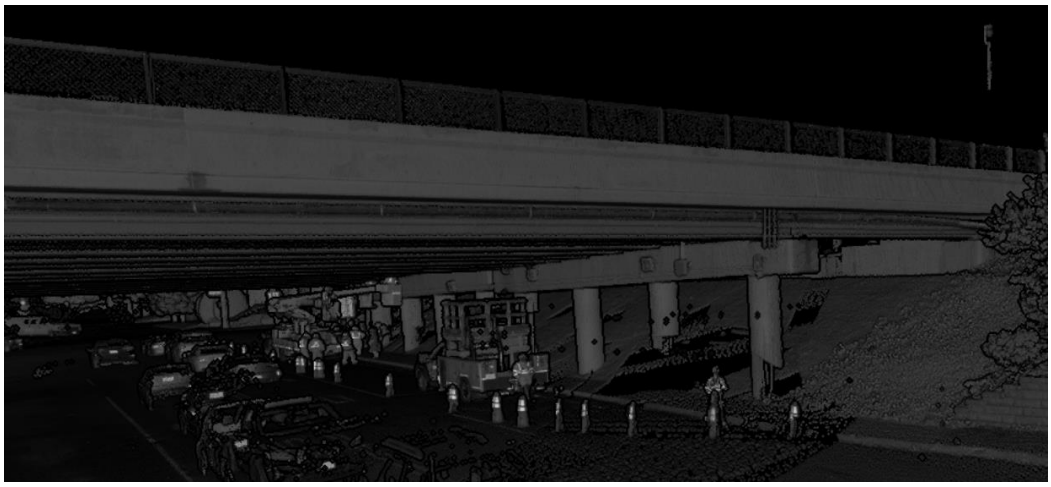

**Figure 4.10: Terrestrial scan of highway bridge.**

The terrestrial scan of the interstate bridge allows for larger-scale measurements to be conducted such as clearance heights, span lengths, and other large geometric features of the structure.

Individual beam end scans performed by the research team were conducted on the typical equipment used by bridge inspectors, which included access by means of foot, ladders, and bucket truck. This was done to best imitate what a bridge inspector would have to do when implementing the scanning technology and protocol. The protocol described in the Implementation and Technology Transfer section is the process the researchers used while scanning the components of the structure. Each of the field beam specimens were photographed by the research team or photographs were provided by MassDOT to determine the beams that would be a priority to be scanned as part of this investigation. Following this documentation and beam selection, all of the beam ends were scanned using the Artec LEO handheld scanner *(70)*.

In all of the following four beam scans, the alignment features of Artec Studio were used with supplemental use of ICP alignment if necessary to bring the two sides of the beam

together. These processes are described in the Research Methodology and Protocol section of this report. In Figure 4.11, Figure 4.13, Figure 4.15, and Figure 4.17, the alignment points used for these field scans can be seen in the scan output (c,d); the field scans were conducted using registration objects created by the research team as described in the Research Methodology and Protocol section of this report.

Regarding the mapped surfaces of the scanned field beams, the research team implemented a new visualization alongside the contour maps used in the laboratory scans. These are what are referred to as corrosion (or section loss) heat maps. The research team found that describing web section loss through heat maps and contour maps was advantageous as the contour map presents a generalized map and shape of the corrosion damage present on the beam end while a heat map shows the entire dataset of points. Additionally, heatmaps can capture critical yet small and localized damage, such as pitting, which a generalized contour map may not generate. A heat map also makes it very easy to find and visualize areas of delamination, where there may be excess debris and rust present on the surface. Each of these maps only presents an area of 4 inches high by about 18.5 inches in length; this is the bottom 4 inches of the web, which is the area of the web that has been found through experiments and analysis to govern the failure of the beam and has been implemented into the current MassDOT procedures *(46-52, 58-63, 55).* Additionally, the 18.5 length was selected to accommodate the maximum possible length necessary for this beam type via the Mass DOT guidelines *(55).* The heat maps and contour maps for all four of the field beam specimens can be found in parts (a) and (b) respectively of Figure 4.12Figure 4.14,Figure 4.16Figure 4.18.

### 4.2.1 Field Beam 1: Span 2, Beam 19 South, Over Pier 1

(a) photograph courtesy of MassDOT

(b) photograph courtesy of MassDOT

(c) scan output

(d) scan output

**Figure 4.11: Field Beam 1**

The photographs for Field Beam 1 in (a,b) were provided by MassDOT as part of a previous inspection. The individual scans for the sides of Field Beam 1 can be seen in (c,d). It is clear here how one side of the beam end exhibits more corrosion than the other. Additionally, the pipe or obstacles in general that impair the vision of the scanner prevent taking a reading on the web where the pipe is present.

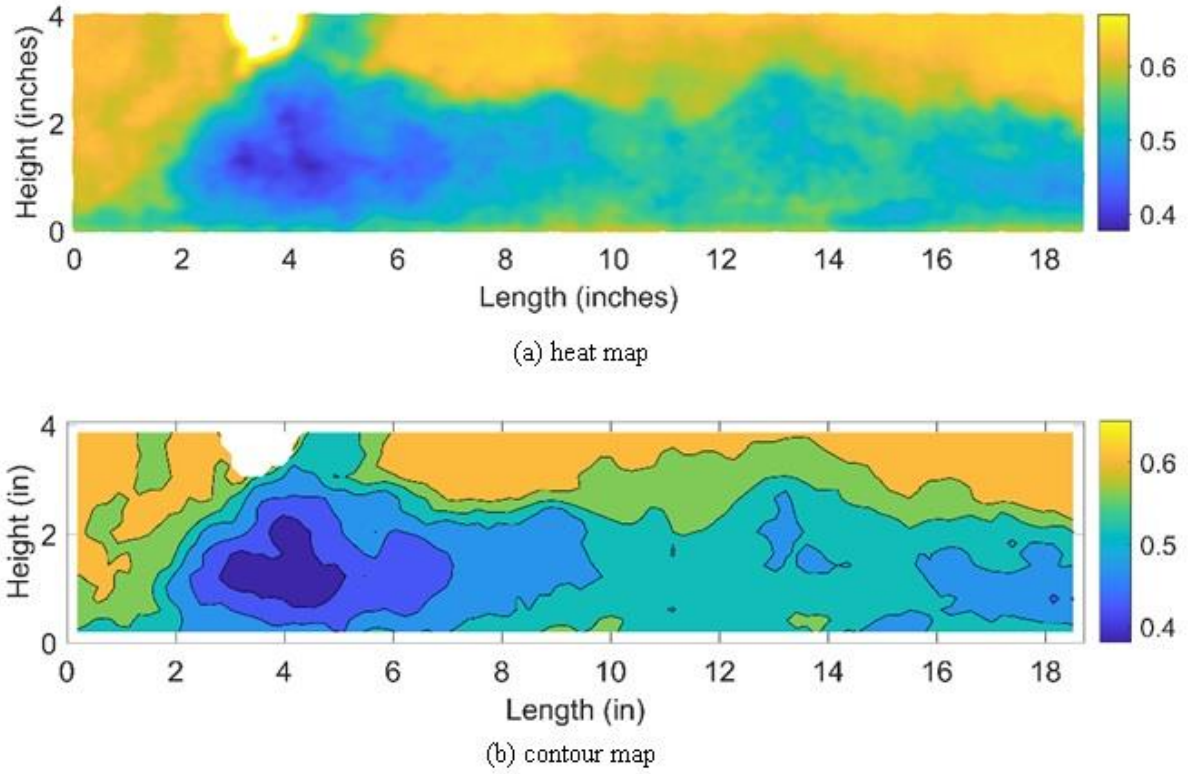


**Figure 4.12: Heat and contour map of Field Beam 1**

The contour map and heat map of section loss shown above for Field Beam 1 show localized and significant damage directly below the stiffener. This circular-shaped region of the most severe web section loss was unique to the beams studied for this bridge.

### 4.2.2 Field Beam 2: Span 2, Beam 20 North, Over Pier 2

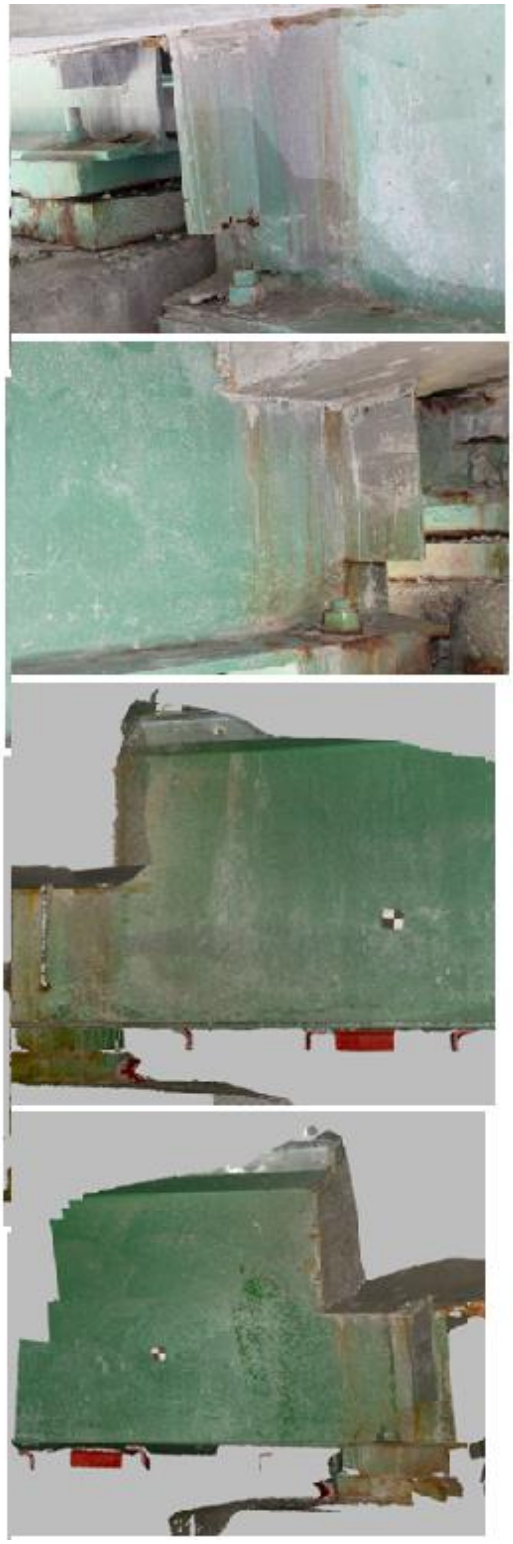

(a) photograph

(b) photograph

(c) scan output

(d) scan output

**Figure 4.13: Field beam 2**

The photographs in (a,b) for Field Beam 2 were taken by the research team. The individual scans for the sides of Field Beam 2 can be seen in (c,d). Visually, there is limited "new" corrosion damage that can be seen in the scan due to a repaint. Although this is the case, the section loss damage is visualized in Figure 4.14.

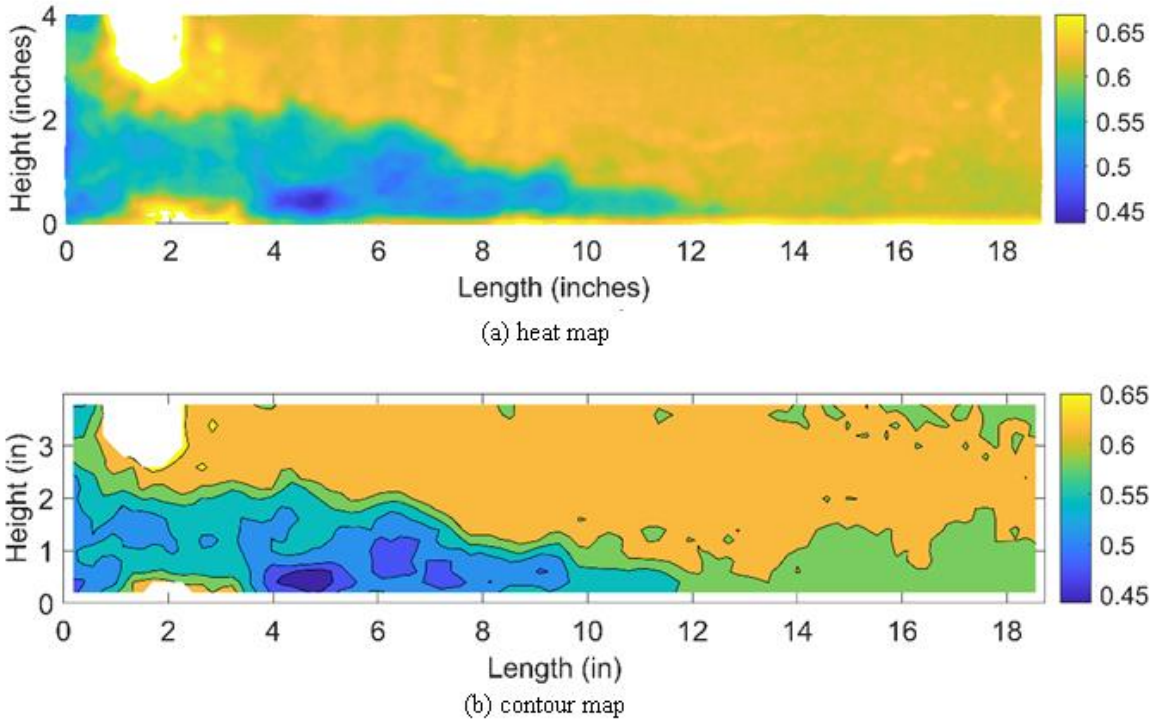


**Figure 4.14: Heat and contour maps of Field Beam 2**

The contour map and heat map of section loss shown above for Field Beam 2 show localized and significant damage directly below the stiffener, but is a long triangular shape that lies just above the bearing. This semi-triangular shape was a corrosion profile that would be expected as water, de-icing chemicals, and other debris typically settle at the base of the web.

### 4.2.3 Field Beam 3: Span 2, Beam 22 North, Over Pier 2

(a) photograph

(b) photograph

(c) scan outputs

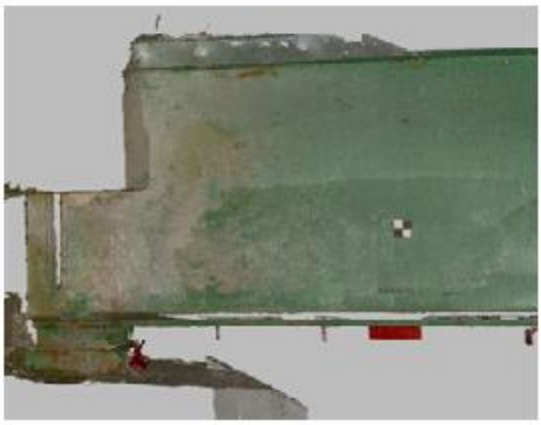

(d) scan outputs

**Figure 4.15. Field Beam 3**

The photographs in (a) for Field Beam 3 were taken by the research team. The individual scans for the sides of Field Beam 2 can be seen in (b). There is limited "new" corrosion damage that can be seen in the scan due to a repaint. Additional debris can be seen on the web around the stiffeners and the concrete diaphragm present. The research team conducted these on-site scans "as is"; therefore, the beam was not cleaned, but the research team advises these areas be cleaned. Additionally, limited debris extended into the base of the web, which was the area of interest for the project. The resulting section loss damage is visualized in Figure 4.16.

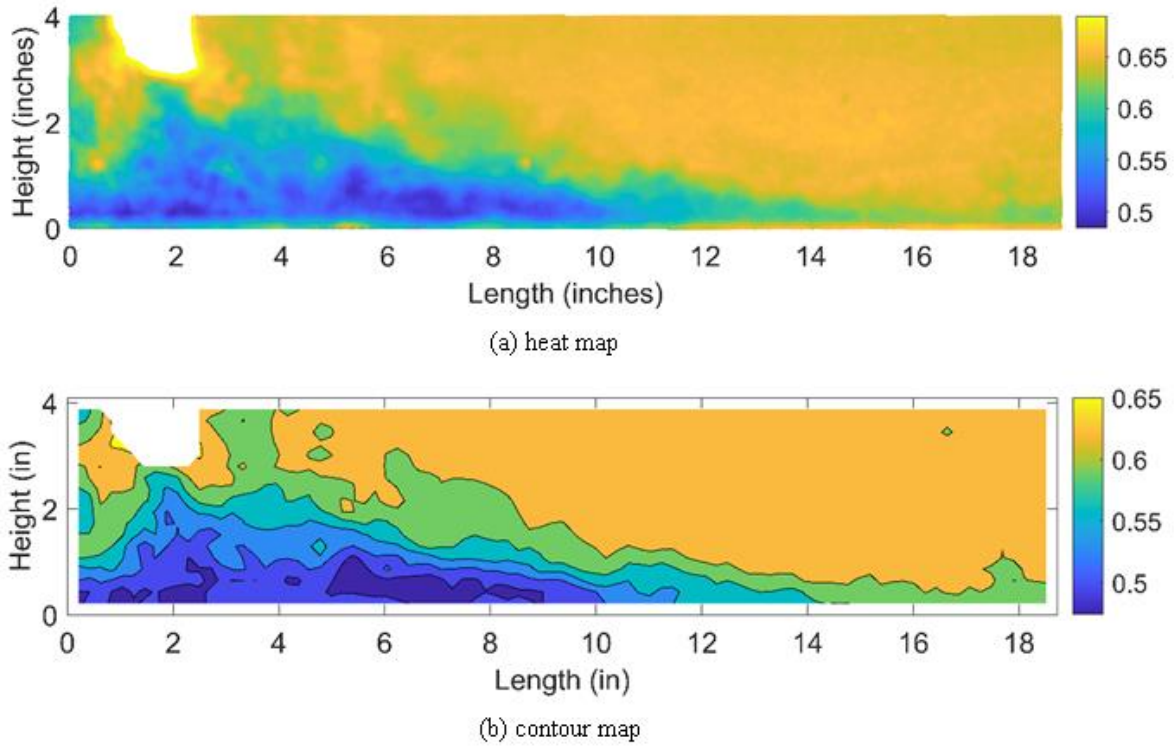


**Figure 4.16: Heat and contour maps of Field Beam 3**

The contour map and heat map of section loss shown above for Field Beam 3 show localized and significant damage directly below the stiffener with a long triangular shape similar to that of Field Beam 2. Again, this corrosion profile is similar to that of Field Beam 2 but differs in severity of section loss.

### 4.2.4 Field Beam 4: Span 2, Beam 31 North, Over Pier 2

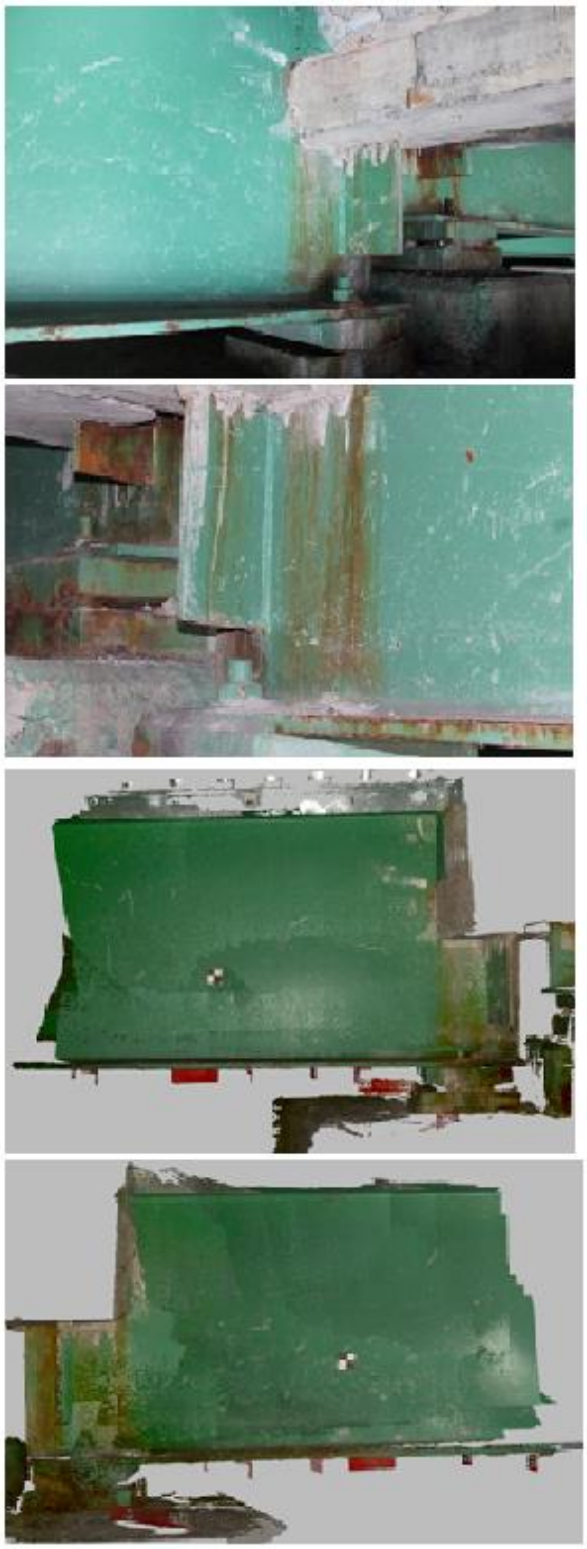

(a) photograph

(b) photograph

(c) scan output

(d) scan output

**Figure 4.17. Field Beam 4**

The photographs in (a,b) for Field Beam 4 were taken by the research team. The individual scans for the sides of Field Beam 2 can be seen in (c,d). There is limited "new" corrosion damage, similar to Field Beams 1 and 2, that can be seen in the scan due to a repaint. There is some rust staining and limited debris below the concrete diaphragm. The resulting section loss damage is visualized in Figure 4.18.

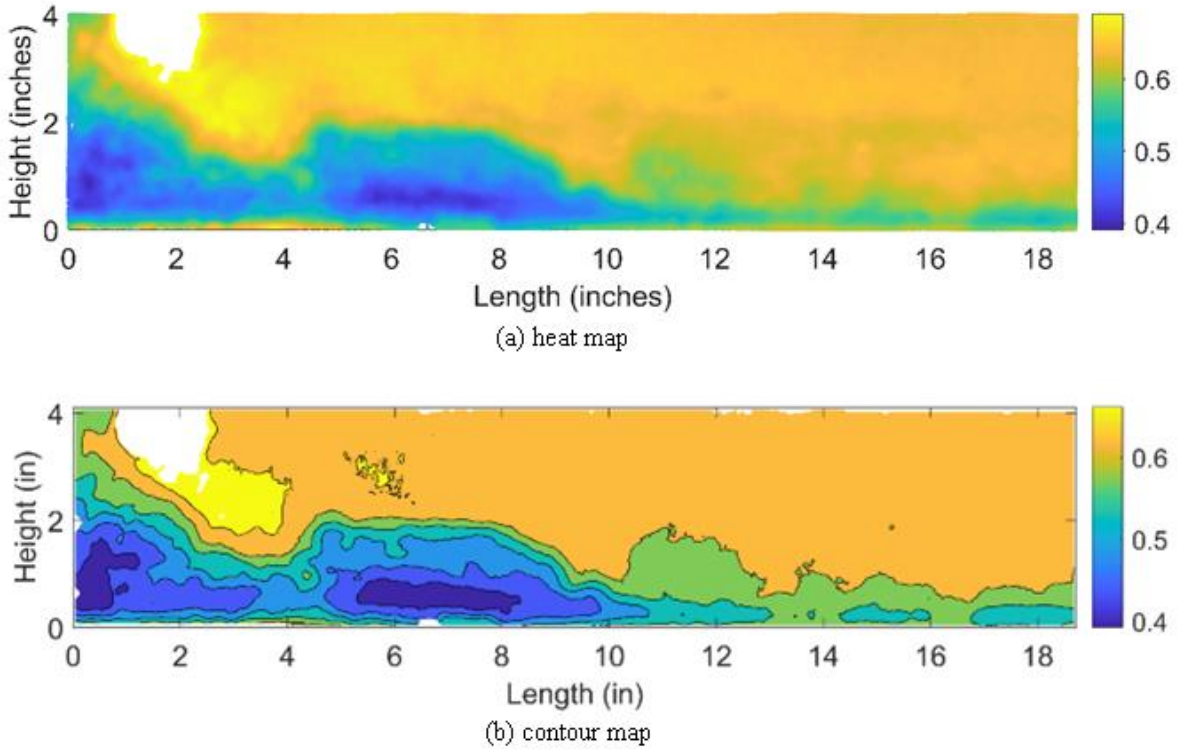


**Figure 4.18: Heat and contour maps for Field Beam 4**

The contour map and heat map of section loss shown above for Field Beam 4 show significant damage in two areas directly below the stiffener with the overarching shape resembling the triangular profile that is similar to that of Field Beams 2 and 3. This profile, while similar to that of Field Beams 2 and 3, differs in severity of section loss, particularly with its two critical areas of maximum section loss.

## 4.3 Validation and Measurements

Rigorous measurements were taken using the PocketMIKE and slide calipers to check the intact thicknesses of the web and flanges. Due to time and access limitations, the grid system created in the lab setting was not created on the beams studied as a part of the field scans. To validate the scans taken on the bridge, the research team took several PocketMIKE readings at multiple locations along the web of representative beams in areas where the thickness was fully intact. Additional ultrasonic thickness readings were taken on the flanges of these

representative beams to help gain more insight into the beam type. The height of the beam was estimated via taking the height from the bottom face of the bottom flange to the bottom of the top flange; this does not account for the thickness of the top flange. As damage was limited and fairly localized to the base of the web on the beams, the intact thickness of the beams was used for cross-checking the scanning results. A key point here is the presence of paint on these beams; while paint is quite thin, it can contribute about 0.02 inches of thickness total when considering both sides of the beam (two layers of paint). This means that the true thickness of the beam is roughly 0.02 inches less in all of the field specimen heat maps and contours shown in Figure 4.12, Figure 4.14, Figure 4.16, and Figure 4.18. The measurements taken by caliper and PocketMIKE also included paint for consistency among all the tools used. PocketMIKE measurements were taken directly on the beam; caliper measurements were obtained by using holes that were previously drilled in the manufacturing of the beams *(67)*.

The measurements conducted with the caliper and PocketMIKE ultrasonic thickness gauge in Table 4.1 were used to validate the field scans conducted as a part of this study *(67)*. This was done to ensure and check that the resulting scans performed in the field were accurately capturing the true remaining thickness of the beam end. As creating a thickness grid and performing hundreds of ultrasonic thickness measurements is very time-consuming and laborious, the research team considered areas of what appeared to be intact thickness of the beams to validate areas of the beam end in the scan without damage. The summarized raw measurements without removing this assumption for paint can be found in Table 4.1.

**Table 4.1: Validation measurements for field beam specimens**

| Beam | Thickness (inches) PocketMike *(67)* | Thickness (inches) Caliper | Global Geometry (inches) Tape Measure |
|---|---|---|---|
| **Representative Beam 1** | **Web:** 0.6501 **Flange Large:** 0.877 **Flange Small:** 0.734 | **Web:** 0.6690 **Flange Large:** NA **Flange Small:** 0.730 | **Height:** 32.25 (without top flange) **Width:** 11.625 |
| **Representative Beam 2** | **Web:** 0.6543 **Flange Large:** 0.8776 **Flange Small:** 0.7340 | **Web:** 0.6591 **Flange Large:** NA **Flange Small:** 0.7286 | **Height:** 32.40 (without top flange) **Width:** 11.688 |
| **Representative Beam 3** | **Web:** 0.6627 **Flange Large:** 0.9242 **Flange Small:** 0.7883 | **Web:** NA **Flange Large:** NA **Flange Small:** 0.8037 | **Height:** 32. 32 (without top flange) **Width:** 11.625 |

*Note, several measurements were taken on each beam in different locations and averaged to be placed in this table

This page left blank intentionally.

# 5.0 Implementation and Technology Transfer

The following document describes a comprehensive implementation and technology transfer via a protocol for bridge inspection methods using 3D scanning. This protocol was developed and tested through laboratory and fieldwork conducted by the University of Massachusetts–Amherst research team (the "research team" hereafter), funded by the Massachusetts Department of Transportation (MassDOT) and the Federal Highway Administration (FHWA).

## 5.1 Scanner

The research team has used several scanners for bridge inspection, including the terrestrial light detection and ranging (LiDAR) system Riegl VZ-2000 and the Artec LEO handheld scanners *(69, 70)*. This beam-end inspection protocol is drafted based on the data collected by the Artec LEO handheld scanner (the "LEO" hereafter) *(70)*. The LEO is a structure-from-motion scanner based in photogrammetry where the device continuously captures high-quality photos and stitches them together; high-quality measurements can be taken with a high-definition option and capture up to a point accuracy of 0.1 mm and 3D resolution of 0.2 mm *(70)*. While high definition is not necessary for quality measurements, it provides greater detail but costs more in storage. For the purposes of beam end corrosion documentation, this accuracy and resolution are considered adequate.

The LEO has a long-lasting battery, making it easy to use for approximately 4 hours of scanning with few breaks and can last longer where scanning is not being performed constantly *(70)*. It is worth noting that hours of battery life vary depending on how much scanning is being performed, if temperature control is being used for normalizing the system temperature (drains about 3 times faster), and if HD mode is being used for higher quality scans *(70)*. The recommended operating temperature is between 59 and 95 degrees Fahrenheit and up to 80 percent humidity but can use the temperature control option for environments not in this range *(49)*. The LEO is equipped with high memory storage (400 GB) for storing many projects from the same inspection *(70)*. The LEO provides a touchscreen on board to display and check the scans performed *(70)*. The full storage of the LEO will sustain an estimate of 80 or more beam ends in non-HD mode and approximately 40 in HD mode *(70)*. These files can easily be transferred via micro-SD cards or Ethernet; in the field, it is possible to transfer files to micro-SD and clear the internal storage for more scans. It is recommended to avoid this and to transfer all the scans when done with the field work for the day if the internal storage proves sufficient for the work being done that day. The LEO's small size and low weight of approximately 5.7 pounds allows for maneuverability and reaching the beam ends on foot if necessary or used in equipment like a bucket truck or snooper (see Figure 5.1) *(70)*.

Left: the LEO scanner *(70)*. Right: an inspector operating the LEO *(70)* and performing a beam end scan from a bucket truck on a highway bridge.

**Figure 5.1: LEO scanner**

## 5.2 Pre-Scanning

Trip planning is the first critical step in the scanning process. It is recommended to have the bridge plans on hand as well as the latest condition documentation for the beam ends of interest from inspection reports. Marking the desired beam ends for scanning on the bridge plans will allow for proper planning regarding access to each beam end. This access is typically on foot, via ladder, or with the use of a bucket truck or snooper, all of which are able to be used in the scanning process. Because many snoopers and bucket trucks involve lane closures, these are the most critical to plan for; planning to scan multiple beams in a row that are on the same pier and require only movement of the bucket truck/snooper would provide a fast and effective scan inspection. Efficient planning can significantly minimize the hours of lane closures for the bridge inspection.

With the amounts of delamination in the form of corrosion and flaking paint, the remaining steel on a corroded girder is difficult to measure. Scanning inspection at this time requires the surface to be cleaned to better capture the section loss profile. A Model 40 DESCO needle gun is recommended to clean corroded beam specimens with a Dominator 6-gallon ULPA filter vacuum and a hammer for larger pieces. The combination of these tools has proven successful in the laboratory setting in clearing the necessary debris for high-quality scan evaluations. The research team recommends cleaning all the corrosion and chipping or bubbling paint for full-scale section loss evaluations of a corroded end.

For capacity estimation of a corroded end and ultimately load rating a bridge structure, the team recommends cleaning both sides of the beam, focusing mostly on the bottom four inches of the web in height and the corrosion length along the web highlighted via the provisions in the MassDOT Bridge Manual *(55)*. Figure 5.2 shows an example of the described area.

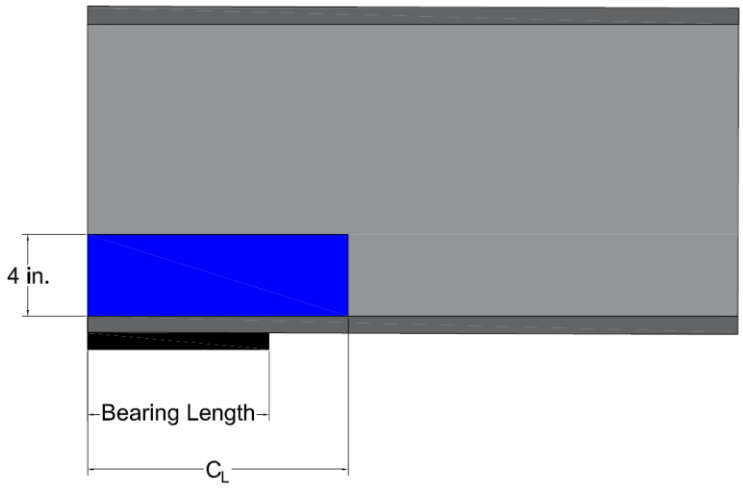


**Figure 5.2. Example area of interest for capacity estimation.**

Prior research conducted by Tzortzinis and established in the newest MassDOT bridge manual describes how the average thickness observed in this area ultimately governs the resulting capacity *(46, 55)*. The Corrosion Length Parameter (CL) is bounded by half of the bearing length to N + md, which is the bearing length plus the depth of the beam times a parameter "m" based on the out-of-web deviation present in the beam end being inspected. Further details can be found in Chapter 7 of the MassDOT Bridge Manual *(55)*.

## 5.3 Setup and Scanning

Additional amenities required for scanning are registration tools or objects, which are objects that are shared by each scan to align the independent sides of a beam end (independent point clouds) into the same coordinate system. Setting up the registration objects is key for the best alignment and to accommodate the variability of scanning situations found due to obstacles and the layout of structures. The principle for placing registration points is to set the objects in all directions in a non-coplanar pattern (i.e., to place registration objects so there is variation in their location in the X, Y, and Z directions) and ideally on either side of the beam end of interest to ensure a better alignment. Proper alignment is critical as errors here can create gross inaccuracy. Registration objects that are the most successful are objects with matte surfaces, unique/diverse textures, and preferably lettering. An example of a registration layout for a corroded end can be found in Figure 5.3.

**Figure 5.3. Registration SEKO *(73)* spheres on a corroded beam specimen.**

Figure 5.3 shows a scanned corroded beam from Maine in a two-side scan scenario. One can observe that the registration spheres are also present and are helpful in the scanning process for object recognition, alignment of multiple scans, and quality checks on the scan.

Scanning distance and speed are also critical for a good-quality scan. The operating distance provided by Artec is 0.35-1.2 meters *(70)*. The scanner provides a filter for observing the optimal distance for a current scan and another filter for observing the quality of the scan being recorded by the operator; this is constantly shown on the screen of the LEO scanner *(70)*. Objects that are too close to the scanner or too far away from the scanner will appear as red and blue, respectfully, when using the filter for distance. The objects out of the scanning range on both the extremely far and close ends of the spectrum (when the scanner is too close or too far from the object of interest) will disappear. The "good" scanning distance described by Artec (0.45 to 0.85 meters in range) appears when the object being scanned is shown as green when the filter for distance is used *(70)*. When using the "quality filter" for scanning, green is described as "well scanned," orange as "satisfactory," and red as "insufficient," which also includes "distant objects" or objects scanned that were captured at too fast of a rate *(70)*. Additionally, changing the angles at which scanning takes place across all surfaces being captured is critical to ensure the object of interest is captured in full detail and high quality. It is relatively easy to read the scan quality during the process without extensive experience, but executing a scanning path will take practice and adjustment for each beam end.

Bridge inspectors and others who will be scanning beam ends should observe the following guidelines for a typical two-sided scan:

- **Pre-Scan Planning:** The beam of interest should be chosen and the scanning plan should be made before getting up near the beam. The plan is especially critical for instances where a bucket truck or other machinery is needed to reach the beam. This will be the most time-consuming task, as making sure the

beam end can be reached may take adjustments, especially if a bucket truck or snooper is being used.

- **Registration Object Placement:** Registration objects, as stated above, should be placed apart from each other in all directions (place registration objects so there is variation in their location in the X, Y, and Z directions) and ideally on either side of the beam end of interest. This configuration will change for each beam end but should be easy to place, especially if the objects can sit on the pier adjacent to the beam or be placed directly on the web via magnets. The registration objects should maintain their positions and poses during the entire scanning session for the area.
- **Scanning Angle and Sequencing:** Scanning should begin when the inspector has placed all registration objects and has a good angle to capture the beam end and the points of interest. A "good angle" for inspectors would be a location where it is easy to capture all the desired web surfaces of the beam end and registration objects. Changing the angles at which scanning takes place is best practice to ensure the object of interest is captured in full detail and high quality. Once the scanning begins, surfaces should be scanned once to avoid making multiple passes on the same surface.
- **Scan Naming Convention:** Each beam end that is scanned should be labeled/named in accordance with the bridge plans used for inspection and/or load rating; this is done by renaming the "project" where the scans are stored. A LEO project stores multiple scans from the same object of interest *(70)*. For example, beam end project naming convention may be the following:

**Span(Number)_Beam(Number)_(Letter for Direction: N, S, E, W)**

An example of the north end of the fourth beam in the first span of a bridge would be labelled as Span1_Beam4_N. NOTE: This is purely a recommendation for the convenience of engineers/inspectors.

- **In-Scan Monitor:** The scanner should be moved with the most consistent pace possible, and not too fast to miss capturing desired web surfaces. If the scanner "loses the object," the scan should be discarded and performed again. Scans should take 1-2 minutes for each side, translating to ~5 minutes for a scanned end. The duration will be slightly longer if multiple scans are taken on either side (recommended). As the system scans, the operator can observe what is being captured and the quality of the scans according to the recommended scanning distance (0.35-1.2 meters), which can be observed in Artec's manual *(70)*. It is best to start the scan in the most desired location for data recording (in the case of corroded ends, this is at the web right above the bearing) and continue traveling in a pattern where the same surfaces are not passed multiple times while ensuring multiple registration surfaces are captured.
- **Post-Scanning Check:** Once the scan is complete, the inspector can stop the scan. The touchscreen on the scanner can now be used to rotate and observe the scan captured. Each scan should be briefly quality-checked to ensure the desired surfaces are captured. This can be done directly via the touchscreen

onboard the LEO; the scan can be rotated to ensure the area of the corroded end and registration objects were captured. This check will only take a maximum of a few minutes per scan and is done purely by a visual check.

- **Redundant Scanning:** To avoid possible scanning errors or unnoticeable missing sections in the scan, it is recommended to take multiple scans of the same area (i.e., scan the same side of the beam multiple times) to ensure all desired points on the beam are captured and to ensure all registration points or surfaces are captured well. Per the In-Scan Monitor section above, these scans would likely take the same time (approximately 1-2 minutes per scan on one side of the beam).

## 5.4 Post Scan Data Alignment

Aligning a two-sided scan is often necessary for on-site measurements. However, there are environments where closed-loop scans could be possible: a scan where both sides of a corroded end can be captured in a single pass. These are typically where inspectors can easily walk under beams near the ends of the bridge at the abutments. An example of this environment on a real bridge can be found below in

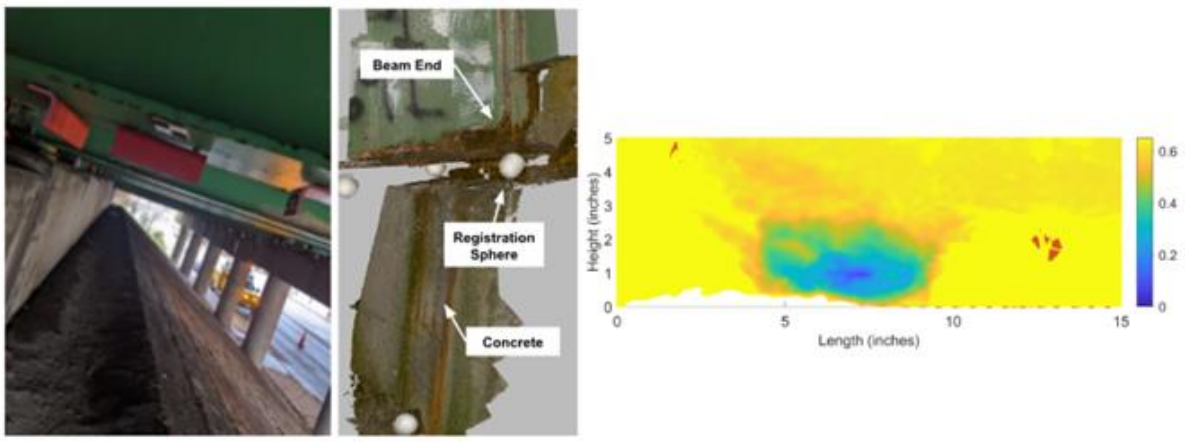


(a) Abutment on a highway bridge accessible by foot, a field environment where a closed-loop scan can be achieved.

(b) Example setup of a beam end scan on a real bridge structure highlighting the corroded end, registration spheres, and the concrete pier surface used for alignment.

(c) A resulting heat map of thickness for the base of the web for a corroded end.

**Figure 5.4: Closed loop scan example**

It is imperative for inspectors who are scanning to capture surfaces shared by both sides of the beam. The easiest surface that both sides of the beam can visualize is concrete, commonly the material used below the beam ends in the form of piers or abutments. The other surfaces would be the alignment/registration points discussed in Setup and Scanning.

The Scanning Center at the University of Massachusetts can receive scans performed by users/inspectors and perform alignment using a combination of software (i.e., Artec Studio and Cloud Compare and codes created in-house for alignment and visualization of the scanning data *(70, 68)*.

## 5.5 Outputs

The outputs can be corrosion (i.e., section loss) contour maps or heat maps, which the University of Massachusetts–Amherst can provide. Contour maps generated for a corroded end allow the inspector to identify the shape of the corrosion. The contour map is created when thickness data is averaged, compiled in a two-dimensional grid, and divided into levels, each of which represents a range of thicknesses. Through the levels of thickness provided, the observer can immediately see the generalized areas created and can pinpoint regions of maximum section loss and the ranges of remaining thickness. Figure 5.5 shows an example contour map of remaining web thickness due to corrosion on a beam end from Maine.

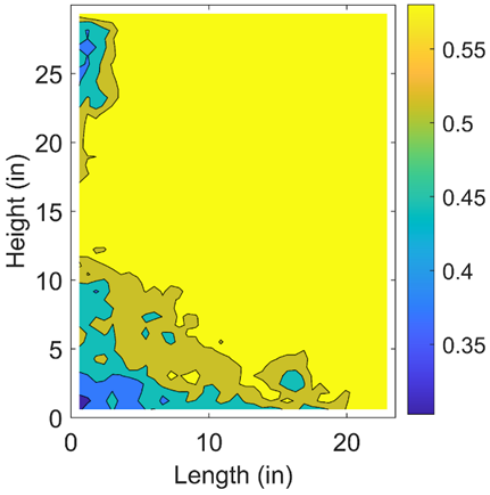


**Figure 5.5: Contour map of remaining thickness (inches) for a corroded Maine beam end**

Similarly, section loss heat maps provide remaining thickness information but are presented through dense point measurements and a color gradient. Mapping section loss through a heat map allows the inspector to observe fine details that the contour map may not provide, such as areas of pitting, holes, and hundreds of thousands of measurement points. The use of the contour and heat maps together has proven very beneficial in evaluating and classifying deterioration as a whole for a corroded beam end. The maps described above can be provided for isolated areas of the beam web or the entire beam web at the corroded end. From this data, the average thickness can also be directly calculated and provided as necessary.

Figure 5.4 (c) shows an example output in the form of a heatmap of the remaining thickness for a beam.

## 5.6 Protocol in Summary

1. **Select Targets of Interest:**
   - Isolate beams/components that will be scanned via inspection reports, bridge plans, and photographs.
   - **Accessibility:** Select how the component of interest will be reached (example: bucket truck/snooper, ladder, by foot).

2. **Plan Scan Path:**
   - Once the component of interest is accessed, it is imperative to make sure all areas to be scanned can be seen by the scanner and reached by the user from the accessibility methods listed above. This can be done by doing a "test run" by holding the scanner and performing test passes without actually scanning the object/surfaces of interest.
   - **Arrangement of Targets:** Place registration objects on both sides of the beam end, varying the placement of individual registration objects as much as possible in the X, Y, and Z directions relative to one another.

3. **Scan Component:**
   - **Begin Scan:** Start the scan pointed at the primary surface that the user wants to be captured (i.e., for corroded ends, the bottom portion of the web where thickness is used for capacity estimation).
   - **Keep Consistent Pace:** The UMass Amherst team recommends that for an area of approximately 3-5 square feet (approximate areas typical for one side of a beam ranging from 16 inches to 36 inches tall), the scan is performed in 1-2 minutes. The user should watch the screen on the scanner to ensure the surfaces being scanned are still being captured and should change the speed of their scanning passes accordingly. Note: some objects/surfaces will require changing the angle and distance at which the scanner is held to ensure sufficient capture (this could slightly increase the scan time noted above).
   - **Scan Technique:** It is recommended not to make several passes on the same surface. These passes refer to scanning a surface of interest, moving to scan other surfaces, and returning to the first surface for a second pass in one scan. Note: this does not refer to changing the angle and distance on a single surface being scanned.
     - Distance Filter: The "good" scanning distance described by Artec is 1.5 feet to 2.5 feet in the range *(70)*. Yellow to red will show "too close" and teal to blue will show "too far." Eventually, if the scanner is extremely close or extremely far from the scanned surface, the surface

will “disappear” or become transparent *(70)*.
    - Quality Filter: Green shows “well scanned,” orange “satisfactory,” and red “insufficient,” which also includes “distant objects” or objects scanned that were captured at too fast of a rate *(70)*.
- **Check Scan When Complete:** Perform a quality check to ensure that the scanned object or surface was fully or sufficiently captured. The object/surface can be rotated and zoomed in or out upon using the touchscreen onboard the LEO *(70)*.

4. **Post Scan:** Back up the scans taken in the field as soon as possible, whether that is on cloud storage (via Ethernet transfer) or a solid storage device like a micro-SD. This will ensure that all the field work has a backup database in case something happens to the LEO scanner or in case a file is accidentally deleted *(70)*.

This page left blank intentionally.

# 6.0 Conclusions

This study allowed for the University of Massachusetts research team to investigate different types of scanning equipment, which included a selection of 3D scanners, several types of registration and alignment patterns and objects, and different software processing techniques. Additionally, the team was afforded the opportunity to use these technologies through laboratory and field tests where a variety of beam types and corrosion profiles could be investigated. The many facets of this study allowed the research team to find what was necessary and best to create a protocol for 3D scanning corroded beam ends for the Massachusetts Department of Transportation. Alongside this protocol, there are several conclusions that the research team have made based on the current research study.

The thickness results of scanning a corroded beam end have previously been described by contour maps of remaining thickness. In addition to these contour maps, the UMass research team found that section loss heat maps proved to be beneficial and captured damage that may not appear on a generalized contour map. This damage could be the small yet critical areas of corrosion-induced pitting or areas of significant delamination. For this reason, the research team concludes that a combination of these maps gives a far more detailed description of the damage present in the corroded beam end than just using a contour map alone. For bridge inspectors, using scanning and scanning results will help better identify the areas of maximum section loss in the beam end; bridge inspectors can only look at one side of a beam at a time and scanning allows the user to combine section loss found from both sides to get the true area, or multiple areas, of maximum section loss. Additionally, the contour maps and heat maps of remaining thickness show far greater detail than typical point measurement tools. Greater detail, accuracy, and a larger amount of data points will lead to higher accuracy in evaluating the capacity of corroded ends when performing inspection and load-rating processes.

The research team compared the scanning performed through conventional hand tools used by bridge inspectors, such as ultrasonic thickness gauges and slide calipers, to new methods using 3D scanning. Conventional tools are key for finding or documenting baseline, or nominal, thicknesses in the beam webs. While this is the case, these tools can prove very difficult to use due to limited access to beam ends and difficulty to operate consistently, and can have significant inaccuracies due to environmental factors such as rust or pitting. The research team wants to emphasize that validation of scanning data through visual inspection of the scanning alignment is an important feature that needs to be used in tandem with the baseline measurements conducted.

Finally, the 3D scanning protocol described throughout and summarized in the Implementation and Technology Transfer section of this report will take minutes for a bridge inspector who has been trained in scanning to complete on selected beam ends. This process will ultimately cut time or maintain the same duration of a typical bridge inspection but increase the confidence and amount of data gathered for the damage on the corroded beam ends. Additionally, it is imperative to note that not all beams on a structure may need to be

scanned. For beams suffering damage that is difficult to evaluate, for beams where bridge inspectors or load raters need more detailed measurement, and for beams that may need to be repaired are where the research team thinks scanning will play the most critical role.

There are several routes that the research team would like to explore for the future work of 3D scanning in the evaluation of bridge components and the global bridge structure. The main area the research team would like to explore is improving and mitigating the errors within the scanning process, which at this time came from alignment and from surface materials like paint, rust, and other delamination.

Additionally, the research team would like to further investigate creating digital twins of structures with a focus on damaged components. Yearly (or more frequent) scans could be completed to track deterioration and the state of the structure over time, allowing bridge engineers to have thorough structural health monitoring in place. This will ultimately give the department of transportation greater insight into which bridges need to be repaired or replaced and will also provide trends to see what bridges will become more critical in future years.

The limitations of this work were primarily due to time constraints. With more time and more specimens, more data could have been collected and more of the future work discussed above could have been explored in the research time interval. The research team will continue to conduct 3D scans of corroded girders and other bridge components and will continue to investigate the topics for the future work discussed above. The University of Massachusetts research team sees 3D scanning playing a critical role in the future of bridge inspection and is confident in the wealth of information and data that 3D scanning will provide to bridge inspectors, load rating engineers, and other bridge engineering professionals.

# 7.0 References


1. ASCE. Bridges. Infrastructure Report Card, American Society of Civil Engineers, 2020, www.infrastructurereportcard.org/cat-item/bridges/. Accessed May 5, 2021.
2. USDOT FHWA. LTBP InfoBridge, 2023. https://infobridge.fhwa.dot.gov/
3. Wandinger, U. Introduction to Lidar. In *Lidar: Range-Resolved Optical Remote Sensing of the Atmosphere*. Springer New York, 2005, pp. 1–18.
4. Weitkamp, C., (ed.), *Lidar: Range-Resolved Optical Remote Sensing of the Atmosphere*. Springer-Verlag New York, 2005.
5. Middleton, W. E. K., and A. F. Spilhaus. *Meteorological Instruments*. University of Toronto Press, 1941.
6. Hulburt, E. O. Observations of a Searchlight Beam to an Altitude of 28 Kilometers. *Journal of the Optical Society of America*, vol. 27, no. 11, 1937, pp. 377–382.
7. Johnson, E. A., R. C. Meyer, R. E. Hopkins, and W. H. Mock. The Measurement of Light Scattered by the Upper Atmosphere from a Search-Light Beam. *Journal of the Optical Society of America*, vol. 29, no. 12, 1939, pp. 512–517.
8. Synge, E. H. XCI. A Method of Investigating the Higher Atmosphere. *London, Edinburgh, and Dublin Philosophical Magazine and Journal of Science*, vol. 9, no. 60, 1930, pp. 1014–1020.
9. Tuve, M. A., E. A. Johnson, and O. R. Wulf. A New Experimental Method for Study of the Upper Atmosphere. *Terrestrial Magnetism and Atmospheric Electricity*, vol. 40, no. 4, 1935, pp. 452–454.
10. Elterman, L. The Measurement of Stratospheric Density Distribution with the Searchlight Technique. *Journal of Geophysical Research*, vol. 56, no. 4, 1951, pp. 509–520.
11. Maiman, T. H. Stimulated Optical Radiation in Ruby. *Nature*, no. 187, 1960, pp. 493–494.
12. Apple. *iPhone 15 Pro and 15 Pro Max Technical Specifications*, 2024. https://www.apple.com/iphone-15-pro/specs/. Accessed August 3, 2024.
13. Riegl. *Riegl Laser Measurement Systems*, 2024. http://www.riegl.com/. Accessed August 3, 2024.
14. Jauregui, D. V., and K. R. White. Bridge Inspection Using Virtual Reality and Photogrammetry. In *Inspection and Monitoring Techniques for Bridges and Civil Structures*, 2005, pp. 216–246.
15. Linder, W. *Digital Photogrammetry* (vol. 1). Springer, Berlin/Heidelberg, Germany, 2009.
16. Schenk, T. *Introduction to Photogrammetry*. Ohio State University, Columbus, 2005.
17. Canon. *Canon DSLR Cameras: Eos Digital Cameras: Canon U.S.A, Inc.*, 2024. https://www.usa.canon.com/shop/cameras/dslr-cameras.

18. Source Graphics, Artec. *Wireless Handheld 3D Scanner: ARTEC LEO: Best 3D Scanning Solutions*, 2024. https://www.artec3d.com/portable-3d-scanners/artec-leo/.

19. Baltsavias, E. P. A Comparison between Photogrammetry and Laser Scanning. *ISPRS Journal of Photogrammetry and Remote Sensing*, vol. 54, no. 2-3, 1999, pp. 83–94.

20. Riveiro, B., H. González-Jorge, M. Varela, and D. V. Jauregui. Validation of Terrestrial Laser Scanning and Photogrammetry Techniques for the Measurement of Vertical Underclearance and Beam Geometry in Structural Inspection of Bridges. *Measurement*, vol. 46, no. 1, 2013, pp. 784–794.

21. Mohammadi, M., M. Rashidi, V. Mousavi, A. Karami, Y. Yu, and B. Samali. Quality Evaluation of Digital Twins Generated Based on UAV Photogrammetry and TLS: Bridge Case Study. *Remote Sensing*, vol. 13, no. 17, 2021, p. 3499.

22. Truong-Hong, L., H. Falter, D. Lennon, and D. F. Laefer. Framework for Bridge Inspection with Laser Scanning. 2016. Retrieved from http://hdl.handle.net/10197/7476

23. Jáuregui, D. V., Y. Tian, and R. Jiang. Photogrammetry Applications in Routine Bridge Inspection and Historic Bridge Documentation. *Transportation Research Record*, vol. 1958, no. 1, 2006, pp. 24–32.

24. Zollini, S., M. Alicandro, D. Dominici, R. Quaresima, and M. Giallonardo. UAV Photogrammetry for Concrete Bridge Inspection Using Object-Based Image Analysis (OBIA). *Remote Sensing*, vol. 12, no. 19, 2020, p. 3180.

25. Jiang, R., D. V. Jáuregui, and K. R. White. Close-Range Photogrammetry Applications in Bridge Measurement: Literature Review. *Measurement*, vol. 41, no. 8, 2008, pp. 823–834.

26. Hackl, J., B. T. Adey, M. Woźniak, and O. Schümperlin. Use of Unmanned Aerial Vehicle Photogrammetry to Obtain Topographical Information to Improve Bridge Risk Assessment. *Journal of Infrastructure Systems*, vol. 24, no. 1, 2018.

27. Molina, A. A., Y. Huang, Z. Zhu, and M. Namian. Comparing the Accuracy between UAS Photogrammetry and Lidar in Bridge Inspections. Conference: Construction Research Congress, March 2024.

28. Bolourian, N., and A. Hammad. Path Planning of LiDAR-Equipped UAV for Bridge Inspection Considering Potential Locations of Defects. In I. Mutis and T. Hartmann (eds.), *Advances in Informatics and Computing in Civil and Construction Engineering*. Springer, Cham, 2019, pp. 545–552.

29. Bolourian, N., & A. Hammad. LiDAR-Equipped UAV Path Planning Considering Potential Locations of Defects for Bridge Inspection. *Automation in Construction*, vol. 117, 2020, p. 103250. https://doi.org/10.1016/j.autcon.2020.103250

30. Bolourian, N., M. M. Soltani, A. H. Albahria, and A. Hammad. High Level Framework for Bridge Inspection Using LiDAR-Equipped UAV. In *ISARC. Proceedings of the International Symposium on Automation and Robotics in Construction*, vol. 34, IAARC Publications, 2017.

31. Jung, S., D. Choi, S. Song, and H. Myung. Bridge Inspection Using Unmanned Aerial Vehicle Based on HG-SLAM: Hierarchical Graph-Based Slam. *Remote Sensing*, vol. 12, no. 18, 2020, p. 3022.

32. Jung, S., S. Song, S. Kim, J. Park, J. Her, K. Roh, and H. Myung. Toward Autonomous Bridge Inspection: A Framework and Experimental Results. 2019 16th International Conference on Ubiquitous Robots (UR), Jeju, South Korea, 2019, pp. 208–211.

33. Chen, S., D. F. Laefer, E. Mangina, S. I. Zolanvari, and J. Byrne. UAV Bridge Inspection through Evaluated 3D Reconstructions. *Journal of Bridge Engineering*, vol. 24, no. 4, 2019.

34. Perry, B. J., Y. Guo, R. Atadero, and J. W. van de Lindt. Streamlined Bridge Inspection System Utilizing Unmanned Aerial Vehicles (UAVs) and Machine Learning. *Measurement*, vol. 164, 2020, p. 108048.

35. DJI - Official Website. *DJI Official*, 2024. https://www.dji.com/

36. Wingtra, 2024. https://wingtra.com/

37. Arun, K. S., T. S. Huang, and S. D. Blostein. Least-Squares Fitting of Two 3-D Point Sets. *IEEE Transactions on Pattern Analysis and Machine Intelligence*, vol. PAMI-9, no. 5, 1987, pp. 698–700.

38. Besl, P., and N. D. McKay. A Method for Registration of 3-D Shapes. *IEEE Transactions on Pattern Analysis and Machine Intelligence*, vol. 14, no. 2, 1992, pp. 239–256.

39. Bales, F. B. Close-Range Photogrammetry for Bridge Measurement. *Transportation Research Record*, vol. 950, 1985, pp. 39–44.

40. Cooper, M. A. R., and S. Robson. High Precision Photogrammetric Monitoring of the Deformation of a Steel Bridge. *Photogrammetric Record*, vol. 13, no. 76, 1990, pp. 505–510.

41. Fraser, C. S., and B. Riedel. Monitoring the Thermal Deformation of Steel Beams via Vision Metrology. *ISPRS Journal of Photogrammetry and Remote Sensing*, vol. 55, no. 4, 2000, pp. 268–276.

42. Whiteman, T., D. D. Lichti, and I. Chandler. Measurement of Deflections in Concrete Beams by Close-Range Digital Photogrammetry. In *Proceedings of the Symposium on Geospatial Theory, Processing and Applications*. Ottawa, Canada, 2002, pp. 9–12.

43. Chen, S. E., W. Liu, H. Bian, and B. Smith. 3D LiDAR Scans for Bridge Damage Evaluations. In *Forensic Engineering 2012: Gateway to a Safer Tomorrow*. 2013, pp. 487–495.

44. Liu, W., S. E. Chen, A. Sajedi, and E. Hauser. The Role of Terrestrial 3D LiDAR Scan in Bridge Health Monitoring. In *Nondestructive Characterization for Composite Materials*. Aerospace Engineering, Civil Infrastructure, and Homeland Security, 2010, vol. 7649, pp. 358–367.

45. Liu, W., S. Chen, and E. Hauser. LiDAR-Based Bridge Structure Defect Detection. *Experimental Techniques*, vol. 35, no. 6, 2011.

46. Tzortzinis, G., S. Gerasimidis, S. Breña, and B. Knickle. *Development of Load Rating Procedures for Deteriorated Steel Beam Ends*. Report 19-008, Massachusetts Department of Transportation Office of Transportation Planning, 2019.

47. Tzortzinis, G. S., B. T. Knickle, A. Bardow, S. F. Breña, and S. Gerasimidis. Strength Evaluation of Deteriorated Girder Ends. I: Experimental Study on Naturally Corroded I-Beams. *Thin-Walled Structures*, vol. 159, 2021, p. 107220.

48. Tzortzinis, G., B. T. Knickle, A. Bardow, S. F. Breña, and S. Gerasimidis. Strength Evaluation of Deteriorated Girder Ends. II: Numerical Study on Corroded I-Beams. *Thin-Walled Structures*, vol. 159, 2021, p. 107216.

49. Tzortzinis, G., B. Knickle, S. Gerasimidis, A. Bardow, and S. Breña. Development of an Analytical Framework for Strength Assessment of Corroded Steel Bridges. In *AISC Global Assets.* National Steel Bridge Alliance.

50. Tzortzinis, G., B. Knickle, S. Gerasimidis, A. Bardow, and S. Brena. Experiments and Computations on Steel Bridge Corroded Beam Ends. Proceedings of the Annual Stability Conference, Structural Stability Research Council, St. Louis, Missouri, 2019.

51. Tzortzinis, G., S. F. Breña, and S. Gerasimidis. *Improved Load Rating Procedures for Deteriorated Steel Beam Ends with Deteriorated Stiffeners.* Report 21-024, MassDOT, 2021.

52. Tzortzinis, G., B. Knickle, S. Gerasimidis, A. Bardow, and S. Brena. Identification of Most Common Shapes and Locations for Beam End Corrosion of Steel Girder Bridges. Transportation Research Board, Washington, DC, 2019.

53. Javier, E. M. Methods for Evaluation of the Remaining Strength in Steel Bridge Beams with Section Losses due to Corrosion Damage. Doctoral dissertation, Virginia Tech, 2021.

54. Javier III, E. M., M. H. Hebdon, and J. T. Provines. *Methods for Evaluation of the Remaining Shear Capacity in Steel Bridge Beams with Section Losses Attributable to Corrosion Damage.* Publication FHWA/VTRC 22-R4. Virginia Transportation Research Council (VTRC), 2021.

55. MassDOT. *2015 Bridge Inspection Handbook*. 2015, May, revised chapters in 2019. Mass.gov.https://www.mass.gov/info-details/2015-bridge-inspection-handbook2023.

56. Hain, A., A. E. Zaghi, A. Kamali, R. P. Zaffetti, B. Overturf, and F. E. Pereira. Applicability of 3-D Scanning Technology for Section Loss Assessment in Corroded Steel Beams. *Transportation Research Record: Journal of the Transportation Research Board*, vol. 2673, no. 3, 2019, pp. 271–280.

57. Truong-Hong, L., and D. F. Laefer. Documentation of Bridges by Terrestrial Laser Scanner. In *IABSE Symposium Report, IABSE Conference Geneva 2015: Structural Engineering: Providing Solutions to Global Challenges*. IABSE, 2015.

58. Tzortzinis, G., C. Ai, S. F. Breña, and S. Gerasimidis. Using 3D Laser Scanning for Estimating the Capacity of Corroded Steel Bridge Girders: Experiments, Computations and Analytical Solutions. *Engineering Structures*, vol. 265, 2022, p. 114407.

59. Tzortzinis, G., S. F. Breña, and S. Gerasimidis. Experimental Testing, Computational Analysis and Analytical Formulation for the Remaining Capacity Assessment of Bridge Plate Girders with Naturally Corroded Ends. *Engineering Structures*, vol. 252, 2022, p. 113488.

60. . Tzortzinis, G., G. Pryor, K. Yadav, S. Gerasimidis, and S. Breña. *Development of Comprehensive Inspection Protocols for Deteriorated Steel Beam Ends*. Massachusetts Dept. of Transportation Office of Transportation Planning.

61. Tzortzinis, G. A Comprehensive Protocol for Inspection and Assessment of Aging Steel Bridges: Experiments, Computations and 3D Laser Scanning of Field Corroded Girders. Doctoral dissertation, University of Massachusetts–Amherst, 2021.

62. Tzortzinis, G., A. Filippatos, J. Wittig, M. Gude, A. Provost, C. Ai, and S. Gerasimidis. Structural Integrity of Aging Steel Bridges by 3D Laser Scanning and Convolutional Neural Networks. *Communications Engineering*,3(1), 106, 2024.

63. Gerasimidis, S., S. Breña, and G. Tzortzinis. Improved Load Rating Procedures for Deteriorated Steel Beam Ends with Deteriorated Stiffeners (Final Report September 2021 [May 2019-September 2021]). Massachusetts Department of Transportation, 2021.

64. Casas, J. R., D. M. Frangopol, J. Turmo, G. Tzortzinis, C. Ai, S. Breña, and S. Gerasimidis. From Point Clouds to Capacity Assessment of Corroded Steel Bridges. In *Bridge Safety, Maintenance, Management, Life-Cycle, Resilience and Sustainability*. Proceedings of the Eleventh International Conference on Bridge Maintenance, Safety and Management (IABMAS 2022), Barcelona, Spain, July 11-15, 2022, pp. 863–870. CRC Press, Taylor & Francis Group, 2022.

65. Kanakamedala, D., J. Seo, A. H. Varma, R. J. Connor, and A. Tarasova. Shear and Bearing Capacity of Corroded Steel Beam Bridges and the Effects on Load Rating. 2023.

66. Bian, H., S. E. Chen, and W. Liu. Error Sources in Processing Lidar Based Bridge Inspection. *International Archives of the Photogrammetry, Remote Sensing and Spatial Information Sciences*, vol. XLII-2/W7, 2017, pp. 455–459.

67. *PocketMIKE Operating Manual*. GE Inspection Technologies, Lewistown, PA, 2004.

68. *CloudCompare Version 2.6. 1 User Manual*. CloudCompare, 2019.

69. *Riegl VZ-2000 Brochure*. Riegl, 2020.

70. *3D Artec Leo User Guide*. 2021.

71. Mathworks. *MATLABVersion (R2021b, R2022a)*. 2024. https://www.mathworks.com/?s_tid=gn_logo.

72. *Artec Studio 17 Manual*. Artec 3D and Source Graphics, 2022.

73. SECO Precision. *Surveying Equipment and Surveying Supplies by SECO in CA*. Seco, 2023. https://www.secoprecision.com/.